Wakefield Calculation for Superconducting TM_{110} Cavity Without Azimuthal Symmetry

Leo Bellantoni
Fermi National Accelerator Lab
Batavia IL 60510 U.S.A.

Graeme Burt
Lancaster University
Lancaster LA14YR U.K.

FERMILAB-TM-2356-AD-E-TD
September 19, 2007
This copy with erratta, additions incorporated

Abstract

The 3.9GHz TM_{110} mode deflecting cavity developed at FNAL has many applications, including use as a longitudinal bunch profile diagnostic, and as a crab cavity candidate for the ILC. These applications involve beams with substantial time structure. For the 13-cell version intended for the bunch profile application, long-range wakes have been evaluated in the frequency domain and short-range wakes have been evaluated in the time domain. Higher-order interactions of the main field in the cavity with the beam have also been parameterized. Pedagogic derivations are included as appendices.

The physical problem

The 3.9GHz TM_{110} mode deflecting cavity developed at FNAL[1] for use in an RF-separated kaon beamline is also useful as a longitudinal bunch profile diagnostic, as a crab cavity candidate for the ILC[2], and in light sources[3]. A normally conducting version is useful for transverse-longitudinal emittance exchange. Unlike the kaon separator application, these uses involve beams with substantial time structure, and the impact of RF energy left in the cavities by such a beam needs to be evaluated.

---

[1] FNAL Technical Memos 2060, 2144; N.Solyak, L.Bellantoni et.al. at LINAC 2004, Lubeck Germany, Aug 2004.
[2] P.Goudket, G.Burt at Snowmass 2005; C. Adolphsen, private communication.
[3] G.Waldschmidt, private communication; A.Zholents, Advanced Photon Source Strategic Planning Meeting, August 30, 2004.

At frequencies above the cutoff frequency for the beampipe, energy may propagate out the beamline. It need not do so however; there can be energy stored in parts of the cavity that are relatively distant from the beampipe and this energy (called "trapped modes") will stay in the cavity for long periods of time. The basic analysis strategy is to handle long lived modes, either above or below cutoff, in a semi-analytic frequency domain method, and to confirm that these are indeed the dominant contributions by doing a numeric time domain calculation. Similar calculations are commonplace for cavities with azimuthal symmetry.

When used as a bunch profile diagnostic, the cavity will reside in a beamline that is used for a number of beam physics studies. If there are optical elements downstream of the cavity, it will be valuable to know what the cavity will do to the beam when unpowered and left at 4.15K. To this end, the calculation allows for the inclusion of an estimate of the surface resistance at various frequencies at 4.15K. The power loss is estimated from the geometry constant $G = Q_0 R_{SURF}$ where R_{SURF} has a frequency-squared dependence. The surface resistance at 4.15K and 3.9GHz is a free parameter; it is set to 6370nΩ, (as determined by fits to DESY data from 1.3GHz TM_{010} cavities) by default.

The TM_{110} π mode is the primary, klystron-powered mode of the cavity. It has transversely deflecting magnetic fields in the center of each cell, and deflecting electric fields in the irises. The phases of the two components cause constructive interference with bunches traveling at the speed of light, and the contribution to the deflection from each source is about equal. At "zero crossing", the head of the bunch sees a deflection in one direction and the tail sees a deflection in the opposite direction. The bunch shape is rotated, or "crabbed", but its direction is unchanged. Additionally, depending on the entrance point, there will be some other, secondary effects on the beam trajectory and energy.

The default beam parameters are set with the initial configuration of the A0 beamline after installation in the NewMuon/SMTF site at FNAL: 337ns bunch spacing, 3.2nC bunches of 1ps length. The upgraded beam energy of 40MV is taken as the default. There are 5 bunch trains per second, and the transverse spot size is about a millimeter. Bunch train lengths will be around 3000 bunches.

The first-phase ILC beam parameters, for the nominal configuration, are[4]: 3.25MHz bunch spacing, 3.2nC bunches of 1ps length. The beam energy is 250GeV, and there are 2820 bunches in a train. There are 5 bunch trains per second, and the transverse spot size at the crab cavities is about (σ_x, σ_y) = (510μm, 34μm) for the 20mrad crossing. For the 2mrad crossing, (σ_x, σ_y) = (1130μm, 35μm) and at the IP, these numbers are (655nm, 5.7nm). The allowed

[4] G.D.E. Baseline Configuration Document, draft of 3 March 2006; Andrei Seryi &Sasha Drozhdin, private communications.

bunch-to-bunch beam jitter in the train (position or angle) at the crab cavity location could be up to about a $\sigma/4$ in both x and y. However, the allowed offset (in position or angle) of the whole train in the crab cavity can be up to several sigmas, and can be random from train to train.

The additional kick from crab cavity need to be small enough so that the bunch-to-bunch jitter at the IP should not increase by much more about $\sigma/10$. The energy change of the bunch due to crab cavity must be less than 2×10^{-5}. That is because these cavities (4 per line, 9 cells each) are in front of the final doublet which has focusing length of about 5m, for a bunch length can be as low as 0.2mm, the shift of focus should be smaller than 0.1mm. The tolerance to wakefields in the crabbing angle are 10nrad horizontally and 0.6nrad vertically.

The frequency domain analysis

The problem is to find the interaction of a bunch train upon a following bunch as mediated through fields that persist inside the cavity. The beam has velocity $c\,\hat{z}$, *i.e.* is exactly parallel the longitudinal (z) axis of the cavity. The longitudinal extent of the cavity is $\pm L$, in the sense that electric boundaries at $z = \pm L$ will not perturb the fields of the resonant modes. With this, integrals over z from $-L$ to $+L$ can be replaced with integrals from $-\infty$ to $+\infty$. The exciting bunch train and the trailing bunch enter the cavity at the same (r,ϕ) value, and with the same charge and with uniform spacing. (For most of the calculation we will carry the positions $\vec{r}_1 = (r_1, \phi_1)$ and $\vec{r}_2 = (r_2, \phi_2)$ as independent variables, along with the charges q_1 and q_2, and call the interbunch distance s.) Space charge effects are negligible in that the charge of the bunch makes a negligible contribution to the electric field, *i.e.*, $\nabla\Phi \sim 0$, and the electric field is generated only by the time derivative of the magnetic potential $\vec{A}$.

The electric boundary condition is $\Phi_{\text{CAVITY WALL}} = 0$. In MKSA units with the Coulomb gauge $\nabla \cdot \vec{A} = 0$, the Maxwell equations are

$$\left\{-\nabla^2 + \frac{1}{c^2}\frac{\partial^2}{\partial t^2}\right\}\vec{A} = \mu_0 \vec{J} - \frac{1}{c^2}\frac{\partial}{\partial t}\nabla\Phi \qquad\qquad -\nabla^2\Phi = \rho \Big/ \varepsilon_0$$

where

$$\vec{E} = -\frac{\partial}{\partial t}\vec{A} - \nabla\Phi \qquad\qquad \vec{B} = \nabla \times \vec{A}.$$

The wake potential is the force upon a trailing bunch entering at $\vec{r} = \vec{r}_2$ created by a leading bunch entering at $\vec{r} = \vec{r}_1$ and s meters ahead of the trailing bunch, normalized to the charges q_1 and q_2:

$$\vec{W}(\vec{r}_1,\vec{r}_2,s)=\frac{1}{q_1}\int_{-\infty}^{+\infty}dz\Big[\vec{E}(\vec{r}_2,z,t)+c\hat{z}\times\vec{B}(\vec{r}_2,z,t)\Big]_{t=(s+z)/c}$$

for $s>0$, and $\vec{W}=0$ for $s<0$ by causality. $\vec{W}$ has dimensions of Ω/s.
The first appendix gives the derivation of the following results for positive s:

1) $$W_{//}(\vec{r}_1,\vec{r}_2,s)=\frac{1}{2}\sum_n\frac{V_n(\vec{r}_1)V_n(\vec{r}_2)}{U_n}\cos\left(\frac{\omega_n s}{c}\right)$$

2) $$\nabla^2_{\perp(1)}W_{//}(\vec{r}_1,\vec{r}_2,s)=\nabla^2_{\perp(2)}W_{//}(\vec{r}_1,\vec{r}_2,s)=0$$

3) $$W_{//}(\vec{r}_1,\vec{r}_2,s)=\sum_n W^{(n)}_{//}(s)\,r_1^m r_2^m\,\cos\Big[m(\phi_1-\phi_n)\Big]\cos\Big[m(\phi_2-\phi_n)\Big]$$

4) $$\vec{W}_\perp(\vec{r}_1,\vec{r}_2,s)=-\nabla_{\perp(2)}\int^s d\sigma\,W_{//}(\vec{r}_1,\vec{r}_2,\sigma)$$

where the two dimensional gradient operator with respect to $\vec{r}_i$ is $\nabla_{\perp(i)}$. The longitudinal integrated accelerating voltage for mode n is $V_n(\vec{r})\equiv\int_{-\infty}^{+\infty}d\xi\left[-i\omega_n\,\hat{z}\bullet\vec{A}_n(\vec{r},z)\,e^{i\omega_n\xi/c}\right]$ where the origin of the ξ axis is selected to make this quantity real; that phases the bunch to the cavity field. The quantities $W_{//}$ and $W_\perp$ are the longitudinal and transverse components of the wakefield, and sums over n are sums over all modes including frequency degeneracies. The convention is that (as there are multiple modes with the same azimuthal order) modes are indexed with n or n', and the azimuthal order of mode n is given by m. A specific set of eigensolutions is required, and U_n and ω_n are the cavity energies and angular frequencies for these modes. Equation (3) is an expansion theorem; $W^{(n)}_{//}$ and ϕ_n are the coefficients of the expansion. It would take a somewhat different form in the case where the cavity does have azimuthal symmetry. Again, we are only considering the long-lived modes; broadband effects are neglected.

To write the specific expansion coefficients for equation (3), define

$$R^{(n)}\!\Big/\!Q\equiv\frac{2}{\omega_n}\frac{\Big\{V_n(\vec{r})\big/r^m\cos\Big[m(\phi-\phi_n)\Big]\Big\}^2}{4U_n}.$$

From equations (1) and (3) directly, we have $V_n(\vec{r})\propto r^m\cos\Big[m(\phi-\phi_m)\Big]$, and so $R^{(n)}/Q$ is independent of $\vec{r}$.

Introducing a term to allow for exponential damping through external couplers, equation (1) gives

$$5)\qquad W_{//}(\vec{r}_1,\vec{r}_2,s)=\sum_n \frac{R^{(n)}}{Q}\omega_n \cos\left(\frac{\omega_n s}{c}\right) e^{\left(-s/c\tau_n\right)}\ r_1^m r_2^m \cos\left[m(\phi_1-\phi_n)\right]\cos\left[m(\phi_2-\phi_n)\right]$$

and then the multipole expansion of equation (3) shows

$$6)\qquad W_{//}^{(n)}(s)=\frac{R^{(n)}}{Q}\omega_n \cos\left(\frac{\omega_n s}{c}\right)\exp\left(-s/c\tau_n\right).$$

For the transverse wake potential, apply equation (4), obtaining

$$\vec{W}_\perp(\vec{r}_1,\vec{r}_2,s)=$$
$$-\int^s d\sigma \sum_n\left\{\frac{R^{(n)}}{Q}\omega_n\right\}\cos\left(\frac{\omega_n\sigma}{c}\right)\exp\left(-\sigma/c\tau_n\right)\ \nabla_{\perp(2)}\left\{r_1^m r_2^m \cos\left[m(\phi_1-\phi_n)\right]\cos\left[m(\phi_2-\phi_n)\right]\right\}.$$

The integral over $d\sigma$ is simplified by $\omega_n >> 1/\tau_n$, leaving

$$\vec{W}_\perp(\vec{r}_1,\vec{r}_2,s)=-\sum_n\left\{\frac{R^{(n)}}{Q}c\right\}\sin\left(\frac{\omega_n s}{c}\right)\exp\left(-s/c\tau_n\right)\ r_1^m\cos\left[m(\phi_1-\phi_n)\right]\times$$
$$m\,r_2^{m-1}\left\{\hat{r}\cos\left[m(\phi_2-\phi_n)\right]-\hat{\phi}\sin\left[m(\phi_2-\phi_n)\right]\right\}.$$

The multipole expansion is then

$$\vec{W}_\perp(\vec{r}_1,\vec{r}_2,s)=\sum_n W_\perp^{(n)}(s)\ r_1^m\left(m\,r_2^{m-1}\right)\cos\left[m(\phi_1-\phi_n)\right]\left\{\hat{\phi}\sin\left[m(\phi_2-\phi_n)\right]-\hat{r}\cos\left[m(\phi_2-\phi_n)\right]\right\},$$

(the factor of m tells us that there is no transverse monopole term) with the expansion coefficient defined as

$$7)\qquad W_\perp^{(n)}(s)=c\frac{R^{(n)}}{Q}\sin\left(\frac{\omega_n s}{c}\right)\exp\left(-s/c\tau_n\right)=-\int^s d\sigma\, W_{//}^{(n)}(\sigma).$$

With these expansions of the wakefield potential in terms of numbers that can be computed with a finite-element analysis, it is possible to compute the impact of the wakefields on a trailing bunch. The energy injected per particle in the trailing bunch is the integral as the bunch passes through the cavity of the longitudinal force of the field: $\Delta E=e\int_{-\infty}^{+\infty} dz\, q_2\left(\vec{E}+c\hat{z}\times\vec{B}\right)_z=q_1q_2W_{//}(\vec{r}_1,\vec{r}_2,s)$, where e = *-1.6* x10^{-19} *C*

for electrons. For the problem at hand, $\vec{r} = \vec{r}_1 = \vec{r}_2$, but we must sum over all the previous bunches in the train, spaced at distances s_i from the trailing bunch:

$$\Delta E(Joule) =$$

$$eq \sum_{bunches} \left(\sum_{n\ monopoles} W_{//}^{(n)}(s_i) + \sum_{n\ dipoles} W_{//}^{(n)}(s_i) r^2 \cos^2(\phi - \phi_n) + \sum_{n\ quadrupoles} W_{//}^{(n)}(s_i) r^4 \cos^2\left[2(\phi - \phi_n)\right] + ... \right).$$

Similarly, angular deflection is given by $\Delta\vec{\Theta} = {eq_2 \vec{W}_\perp(\vec{r}_1, \vec{r}_2, s)} \Big/ {E_0}$, summed over the previous exciting bunches:

$$\Delta\vec{\Theta} = \frac{eq}{E_0} \sum_{bunches} \left(\begin{array}{l} \sum_{n\ dipoles} W_\perp^{(n)}(s_i) r \cos(\phi - \phi_n) \left\{ \hat{\phi} \sin(\phi - \phi_n) - \hat{r} \cos(\phi - \phi_n) \right\} \\ + \sum_{n\ quadrupoles} W_\perp^{(n)}(s_i)\, 2r^3 \cos\left[2(\phi - \phi_n)\right] \left\{ \hat{\phi} \sin\left[2(\phi - \phi_n)\right] - \hat{r} \cos\left[2(\phi - \phi_n)\right] \right\} + ... \end{array} \right).$$

This is the angular deflection seen by the bunch centroid; it is not the crabbing angle due to wakefield excitation. That is determined by evaluating $\Delta\vec{\Theta}$ at the head of the bunch and comparing it to the value at the center of the bunch.

In the case which applies here, where we assess $\phi_n = 0$ dipole modes distinctly from $\phi_n = \pi/2$ dipole modes, but are letting the $\phi_n = 0$ quadrupole terms have the same $R^{(n)}/Q$ values for both the $\phi_n = 0$ and $\phi_n = \pi/4$ modes, these expressions simplify if we write them in an ad-hoc mix of rectangular and cylindrical coordinates, and use eV rather than J as the unit of energy:

$$\Delta E = q \sum_{bunches} \left(\sum_{monopoles} W_{//}^{(n)}(s_i) + \sum_{\phi_n = 0\ dipoles} W_{//}^{(n)}(s_i)\, x^2 + \sum_{\phi_n = \pi/2\ dipoles} W_{//}^{(n)}(s_i)\, y^2 + \sum_{quadrupoles} W_{//}^{(n)}(s_i)\, r^4 \right)$$

and

$$\Delta\vec{\Theta} = \frac{q}{E_0} \sum_{bunches} \left(\sum_{\phi_n = 0\ dipoles} W_\perp^{(n)}(s_i)\, x\{-\hat{x}\} + \sum_{\phi_n = \pi/2\ dipoles} W_\perp^{(n)}(s_i)\, y\{-\hat{y}\} + \sum_{quadrupoles} W_\perp^{(n)}(s_i)\, 2r^3\{-\hat{r}\} \right).$$

The frequency domain calculation

The values of the eigenmode frequencies, $R^{(n)}/Q$ quantities and G values were computed with the finite element package MAFIA.

First I found the spectrum of modes with periodic boundary conditions for a single cell with phase advances of 0, 30, 60, 90, 120, 150 and 180 degrees, up to 16GHz. The mesh had 130 lines in r, and 80 in z, where the z range went from

4.880 GHz for TE_{11} evanescent wave in beampipe
6.375 GHz for TM_{01} "
8.096 GHz for TE_{21} "
10.157 GHz for TM_{11} "
11.137 GHz for TE_{31} "
14.132 GHz for TE_{12} "

Table 1. Cutoff frequencies for 36mm diameter beam pipe.

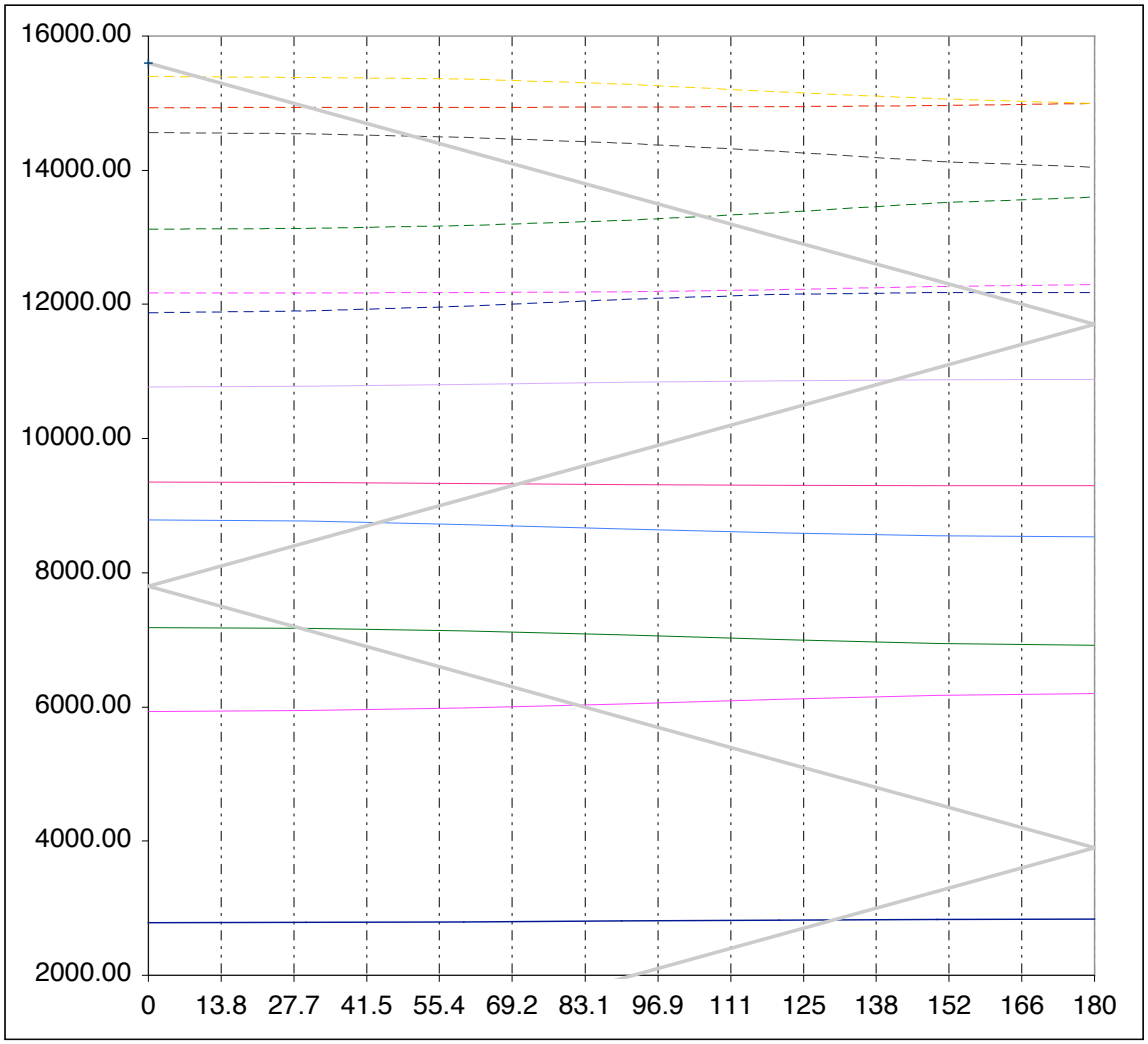

Figure 1. MAFIA periodic-boundary simulation for m = 0 modes.

the equator of one cell to the equator of the next cell, and ϕ ranged over a full 360 degrees. The beampipe cutoffs are in table 1. In all the eigenfinding algorithms, azimuthal dependence is explicitly assigned in the code.

Figures 1 through 3 show the dispersion curves for these three azimuthal numbers; for m = 0, only modes generated with the TM flag set in MAFIA are shown, as TE modes all have zero $R^{(n)}/Q$ anyway.

These curves are useful indicators of where one might expect to find problem modes; when the dispersion curve corresponds to modes with a phase velocity. close to the speed of the bunches, the beam can strongly excite the cavity and vice versa. The phase advance of the intersection is relevant for assessing the value of reducing the number of cells to reduce beam-cavity interactions. This

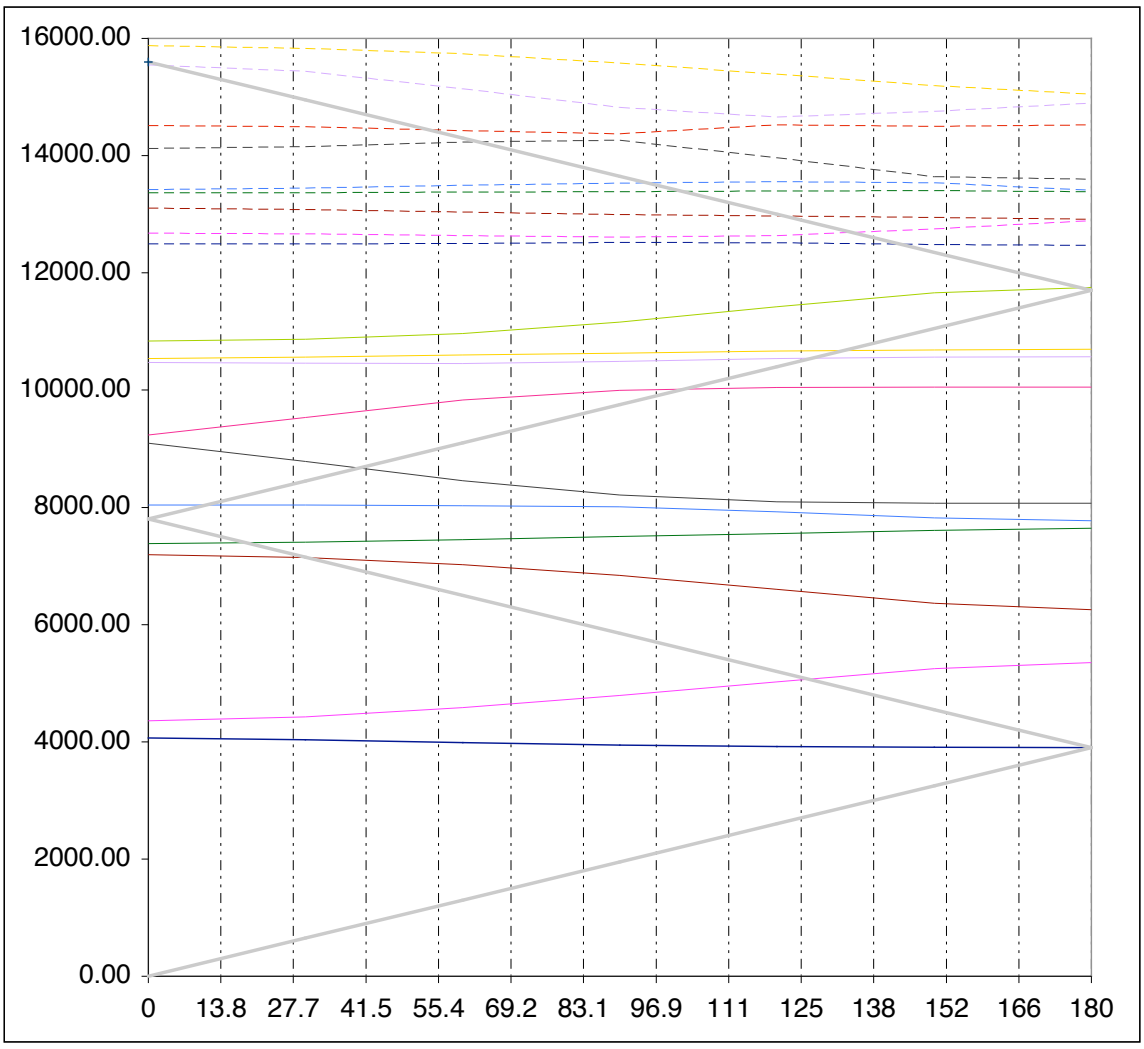

Figure 2. MAFIA periodic-boundary simulation for m = 1 modes.

method is not entirely reliable however; it does not consider $R^{(n)}/Q$ values, *i.e.* the shape of the field and how it interacts with a beam traveling at given β along the cavity axis. Also, a finite structure has slightly different shapes in the end cells, and there will be modes with energy concentrated there. If there are cells with basically zero energy in between, the two end cells need not be phased relative to each other and the structure will not provide cancellation. Modes with low $R^{(n)}/Q$ often do not have low $R^{(n)}/Q$ because there is little beam-cavity coupling in each cell. Rather, the beam-cavity coupling is the sum of beam-cell couplings that can cancel.

Intersection points as determined by linear interpolation, are given in table 2.

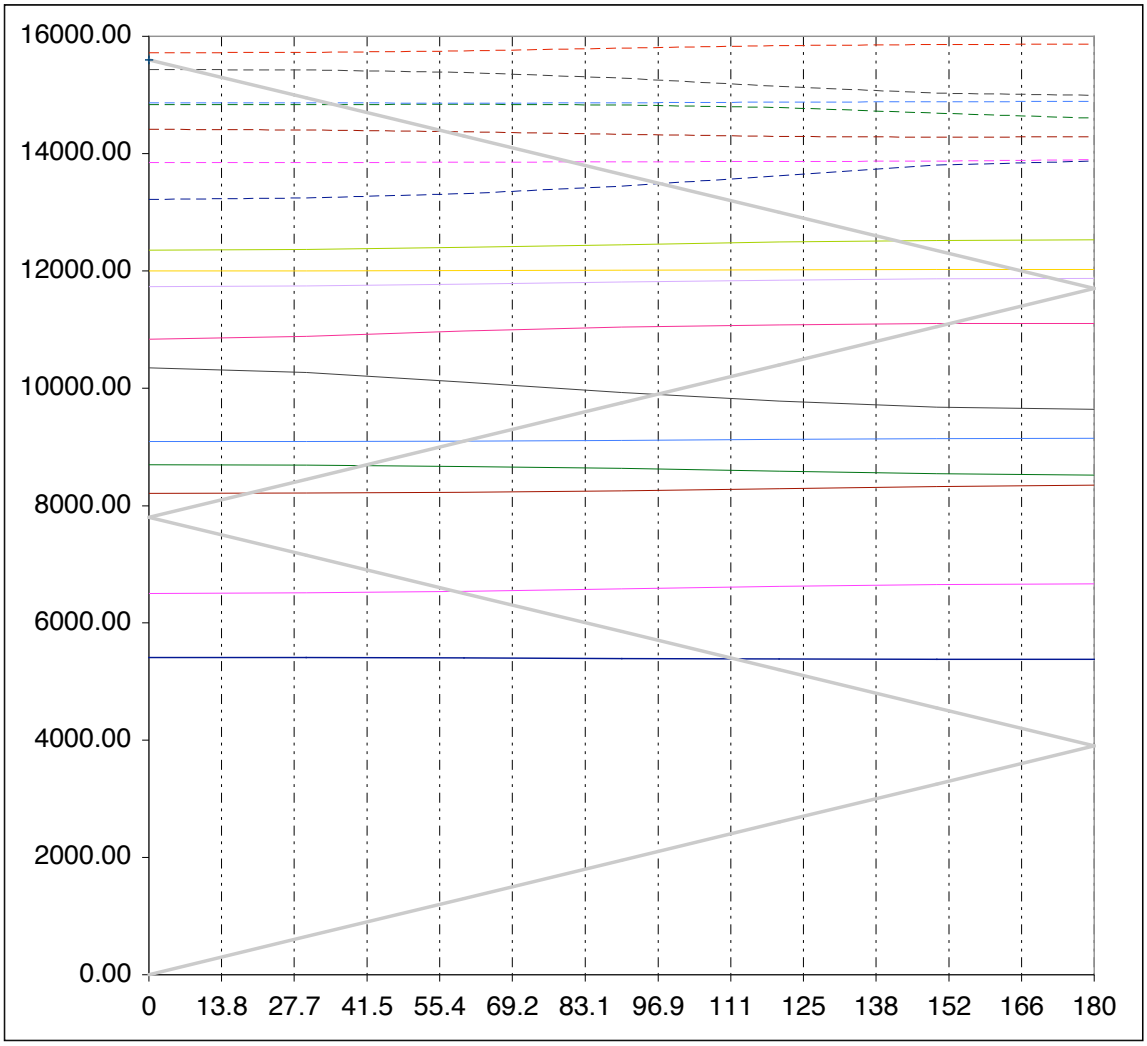

Figure 3. MAFIA periodic-boundary simulation for m = 2 modes.

$m = 0$		$m = 1$		$m = 2$	
ϕ	f (MHz)	ϕ	f (MHz)	ϕ	f (MHz)
130	2826	126	5069	111	5385
82	6029	30	7143	58	6535
29	7173	19	7397	19	8213
44	8747	11	8038	41	8682
70	9324	40	8672	60	9103
142	10871	102	10016	97	9895
158	12173	127	10543	152	11103
154	12271	133	10674	172	11870
106	13313	178	11744	165	12026
50	14509	144	12490	142	12514
31	14935	134	12692	97	13490
9	15397	121	12968	80	13857
		102	13392	57	14374
		95	13538	35	14838
		63	14237	34	14866
		54	14440	8	15431
		3	15542	5	15718
		12	15861		

Table 2. Frequencies and phase advances for intersections of periodic structure dispersion curves with the light cone.

To find $R^{(n)}/Q$ and G values for a finite 13 cell structure the cavity with 0.5m beampipes was simulated using both EE and BB boundary conditions. Variable meshing in the r-z plane was selected so as to allow for the small difference in equator radius between the central and end cell, and to reduce computation time by having relatively few mesh points in the beam pipe. There are 67 mesh lines in r, 719 in z, and a total of 48173 mesh points in the grid. In the beam pipes, the z spacing of the mesh is 4.167mm per line. The double precision version of the eigenfinder was run, and 40 iterations were required.

For m = 0, modes up to 12GHz were found; beyond that the band structure of the periodic single simulation was gone. For m = 1, modes up to 13GHz were found; for m = 2, modes up to 9GHz were found.

To identify and discard modes where there is a lot of energy in the beampipe, a plot of a simulated beadpull of a round metal bead, 5mm off axis at 22.5 degrees was made for each mode. Figure 4 shows such a plot for the main deflecting mode; in this case the significance of the plot is also to show that the meshing reasonably allows for the small difference in equator radii. Were that to not be

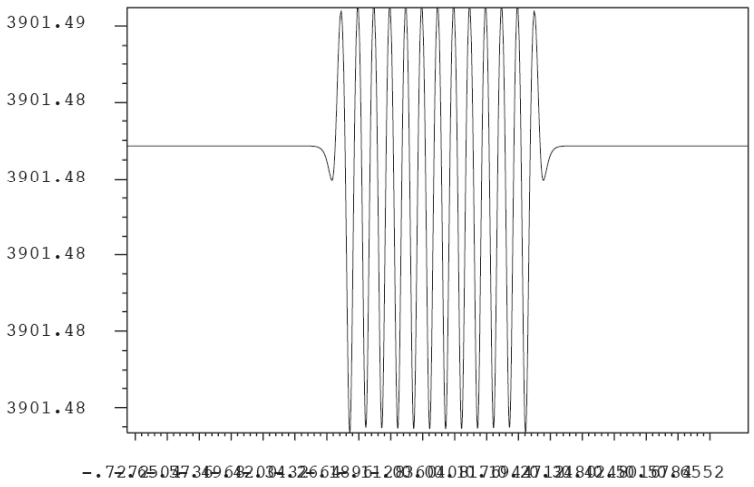

Figure 4. Simulated on-axis bead pull for TM_{110} π mode. The field in the end cell is about 99% of that in the center cell.

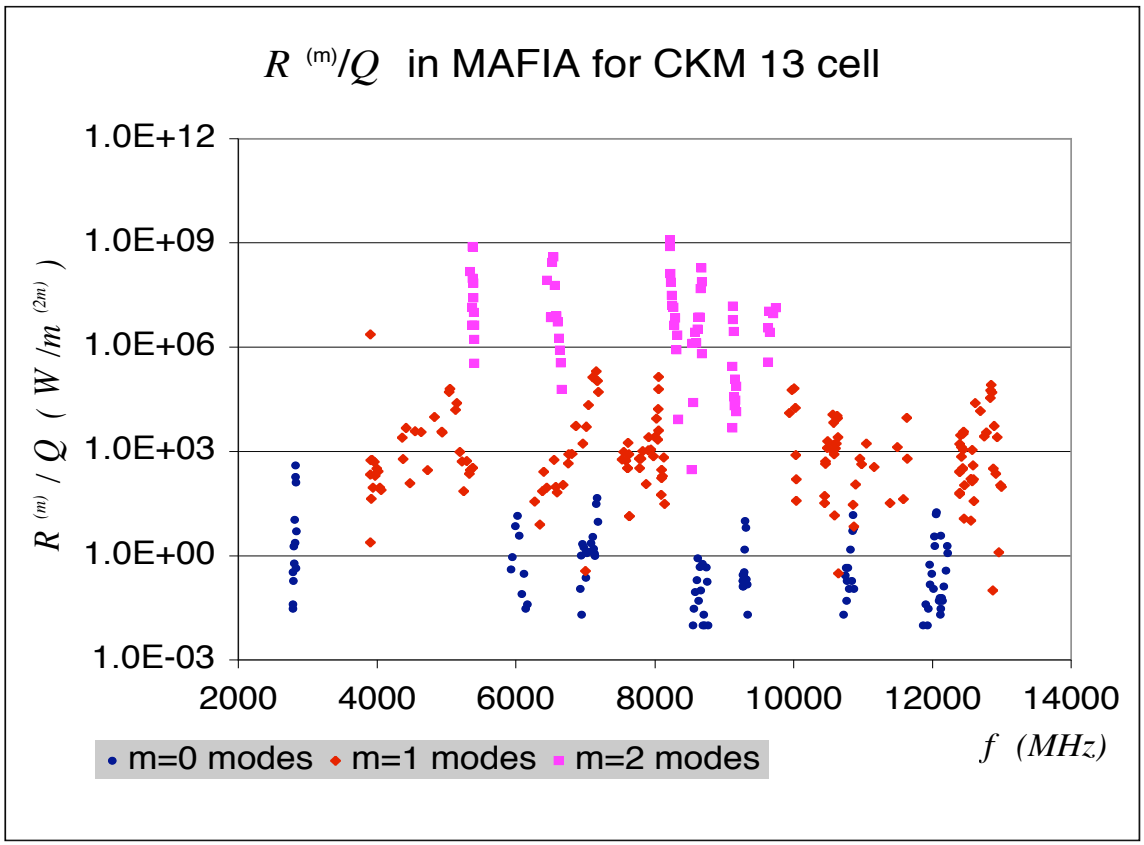

Figure 5. $R^{(n)}/Q$ vs. f in MAFIA for 13 cell TM_{110} mode cavity.

the case, the field uniformity between the cells would be quite poor and the values of $R^{(n)}/Q$ unreliable. These plots were used to see how much energy was in the beampipe and to select the numbers from either the EE or BB boundary condition solution depending upon which had less energy in the pipe. Some subjective judgment was involved in selecting MAFIA solutions from all the outputs of the eigenfinder; this topic will be revisited in the time domain analysis. In the end a total of 346 modes were kept, not counting the multiple degeneracies of the multipole modes.

Figure 5 shows the resulting values of $R^{(n)}/Q$, in units of Ω for m = 0, Ω/m^2 for m = 1, and Ω/m^4 for m = 2. Comparison with an HFSS calculation not reported on here[5] revealed that with such closely spaced modes in so many dispersion curves, having the correct field flatness (as was ensured for these MAFIA runs and meshes) will have a large effect upon $R^{(n)}/Q$ values. The $R^{(n)}/Q$ numbers are sensitive to field flatness because if the cells are slightly different, the fine-tuned cancellation of the individual cell's contribution to the structure's $R^{(n)}/Q$ falls apart. But in the worst case, $R^{(n)}/Q$ in any such mode cannot be as bad as the worst $R^{(n)}/Q$ for that band.

A thorough attempt to model manufacturing defects has not been made. The close mode spacing (only 1MHz near the TM_{110} π mode) does create sensitivity to manufacturing defects. ***This is probably the least reasonable assumption in this study.***

A free parameter for the mode splitting, with a default value of 10MHz was used for the TM_{110} π mode. An ad-hoc formulation was also made for this $R^{(n)}/Q$ value; the additional frequency change was treated as being the same as using a beam with velocity slightly less than one. A 10MHz polarization shifts the frequency to 3910MHz, and a bunch that would have traversed the entire 13 cell cavity in (13/2) times the base period of 256.4ps will instead have traversed (3900/3910) = 99.74% of the cavity in (13/2) times 256.4ps. In effect, the beam has β = 0.9974.

The MAFIA solution for the TM_{110} band gives a π mode at 3.90148GHz; 1.48MHz were subtracted from this and all the TM_{110} solutions.

For the quadrupole bands, the modes were taken to be pinned to the cavities' symmetry-breaking mechanical features, so ϕ_n was either 0 or $\pi/4$.

A spreadsheet that uses the formulas and the outputs of the MAFIA runs described above to determine the impact of the wakefields on the beam is available. Beam parameters are adjustable inputs, including the position of the beam relative to the cavity center. Also adjustable are the values of Q_{EXT} from

[5] I. Gonin, private comunication.

both the main and the damping couplers, and the surface resistance at 4.15K for 3.9GHz. The latter is used to determine a contribution to the damping from surface resistance, should a flag to do so be set. There is also a flag to determine whether or not one should include the non-important modes as described in the time domain analysis.

The spreadsheet calculates ΔE and $\Delta\vec{\Theta}$ as a function of bunch number in the train. Beam breakup condition, where the magnitude $\Delta\Theta$ increases without limit with bunch number, is readily identified.

The π TM_{110} mode

The computed results are compared with the impact on the beam made by the primary π TM_{110} mode. In this section, some higher-order effects on the bunch from the this field are summarized.

The crabbing angle from the primary field is given on the spreadsheet as the deflection angle of the head (or tail) of the bunch relative to the line followed by the longitudinal center of the bunch, which sees net zero deflection due to it's phasing.

There is a longitudinal electric field in the π TM_{110} mode when not in the y-z plane[6], that is 90° out of phase with the deflecting magnetic field. A zero-crossing phase has the bunch passing through the center of the cell as the magnetic field goes through zero, so the bunch will see a change in energy. Also there will be some dispersion introduced to the beam through this effect and the finite span of the bunch in both the z direction and the r-ϕ plane. MAFIA evaluations of E_z, integrated along the length of the cavity, show that at 5MV/m deflection, this energy shift is proportional to the distance of the beam from the axis:

8) $$\int_{-L}^{+L} E_z\left(r = x\right) e^{i\omega z/c} dz \cong (0.204\,MV/mm)\; x$$

This quantity is also given by the spreadsheet.

The loss of power to the beam is a key restriction on the external Q of the power coupler. That is because for the beam on a certain side of the deflecting plane,

[6] In the spreadsheet, in MAFIA, and in the formulas given here, the deflection produced by the lower-frequency π TM_{110} mode is in the x-z plane.

the beam puts energy back into the cavity, and the sharp fluctuations in the required power due to fluctuations in the beam position can be problematic for the power supply.

In the steady state[7],

$$U = \frac{4P_f}{\omega}\frac{Q_{EXT}Q_0^2}{\left(Q_{EXT}+Q_0\right)^2}$$

where P_f is the energy flow out of the klystron. Re-write this in terms of power into the cavity and power into the coupler, and then add to these two power terms $P_{BEAM} = (q_{BUNCH})(f_{BUNCH})(204kV/mm)(x) = \alpha x$, and get

$$P_f = \frac{P_0}{4\beta}\left(1+\beta+\alpha x/P_0\right)^2.$$

When x<0, cancellation, corresponding to no power needed, can occur. Figure 6 shows the klystron power as a function of Q_{EXT} for a range of beam positions. This is for a single cavity operating at 6MV/m deflecting field with surface resistance of 100nΩ. The plot suggests that we want Q_{EXT} on the order of 5 x10^5 for the TM_{110} π mode for the ILC beam, in which the position of the beam train in

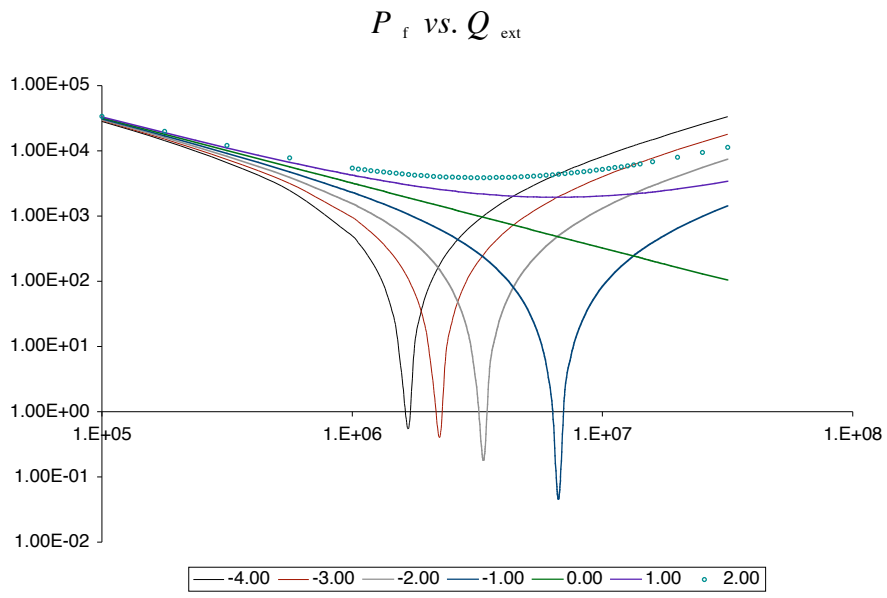

Figure 6. Klystron power requirements vs. Q_{EXT} for a range of beam train offsets.

[7] H. Padamsee, J. Knobloch and T. Hayes, "RF Superconductivity for Accelerators" Wiley Interscience (1998) Equation 8.48

the cavity aperture can vary greatly from bunch train to bunch train. For the beam slice experiment, one can contemplate Q_{EXT} on the order of 1.5 x10^7 if the cavity – beam alignment can reliably keep x in the range 0.0mm to +0.5mm. As iris centers in 3rd harmonic 3.9GHz cavities have an R.M.S. on the order of 0.25mm, this is an aggressive spec.

There is also a sideways slew, meaning that the center of the bunch is displaced in the x direction although its direction and shape are unchanged. This is due to non-zero E_{x} and B_{y} as the bunch is roughly at the 1/4 and 3/4 points of its journey through each cell. The contributions at the 1/4 and 3/4 points have equal and canceling effects, but in between these points, the direction of the bunch's motion is not parallel to the axis. Integration of the MAFIA field plots provides the useful rule Δx = 1.240mm • (Number of cells)/(Beam energy in MeV). So for a 13 cell cavity in a 40 MeV beamline, the slew is 0.4mm; for a 9 cell structure at 250GeV, the slew is about 40 microns. These too are calculated by the spreadsheets.

Note added September 2007: The slew also appears in the beampipes as a result of the evanesecent field. Reviewing the work of E. Branlard in using ASTRA to trace particles through a 5 cell cavity modeled by HFSS, it appears that that this slew is about 3.96mm / (Beam energy in MeV).

The 3-d time domain calculation

Direct numeric integration of the Maxwell equations in the time domain provides a valuable check of the frequency domain study. Has one perhaps missed an important mode that exists well above cutoff? Or conversely, has the subjective selection of modes with a moderate amount of beampipe energy introduced terms in the $R^{(n)}/Q$ expansion that really should not be kept? However long or finely meshed 3D time domain simulations are notoriously compute expensive, and one can not easily adapt the result to the case where a new coupler design changes Q_{EXT}. On the other hand,

Figure 7 shows the electric field of a bunch as it propagates through the cavity. The beampipes are 100mm in length and are terminated with the "waveguide" condition: "The boundary plane is treated as an open boundary for the transversal electromagnetic field of the beam. The parts of the remaining field that are not propagating at the velocity of light are reflected at the boundary plane." The cavity walls have infinite conductivity.

In order to separate the different polarizations, an effect not directly modeled in the frequency domain analysis, and to allow for variations in ϕ of the beam location, a three dimensional model was created. The polarization flats were

located on the $\pm y$ direction, so that the main deflecting mode introduces deflection in the $\pm x$ direction. In MAFIA, this modeling must be done with x-y-z meshing; time domain simulation also requires uniform z meshing. Memory requirements limited the mesh size in z to 1mm; with this in mind, the mesh in x and y are also 1mm. That means that the end cell compensation is not modeled. It also means that the output, W_z, is evaluated at intervals of 3.335ps, (although internally, steps of 1/3 that size are used) and that the Fourier transform of W_z will reach up to 150GHz.

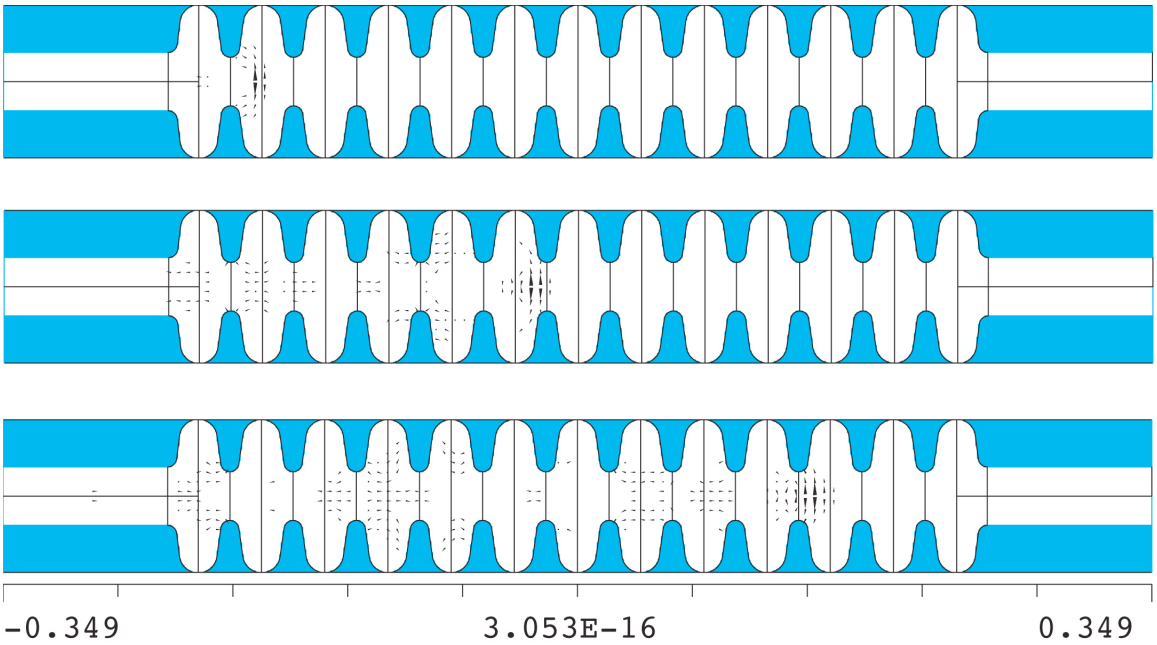

Figure 7. Snapshots of electric field as a bunch progresses through the cavity.

The simulations used the "1dcurrent" method developed by Martin Dohlus[8] and, unless otherwise specified, the Gaussian pulse was 20ps = 6mm wide. Because the endport diameters are larger than the smallest diameter of the structure, the "direct" method of integration was used for the most part. Cross-checks with the "indirect" method will be shown below. Double precision was used.

The first goal of the time domain analysis was to search for trapped modes that were inadvertently missed in the frequency domain analysis. For this purpose a frequency resolution of about 50MHz was deemed sufficient. With the given step size, that entails a computation of $W_z(s)$ for s out to 6 meters. One long run of 20m in s was done, and is shown in figure 8. A 6 meter run is not long enough for the exciting conditions to die down fully, but is enough to show which modes are significant.

[8] Rainer Wanzenberg, private communication.

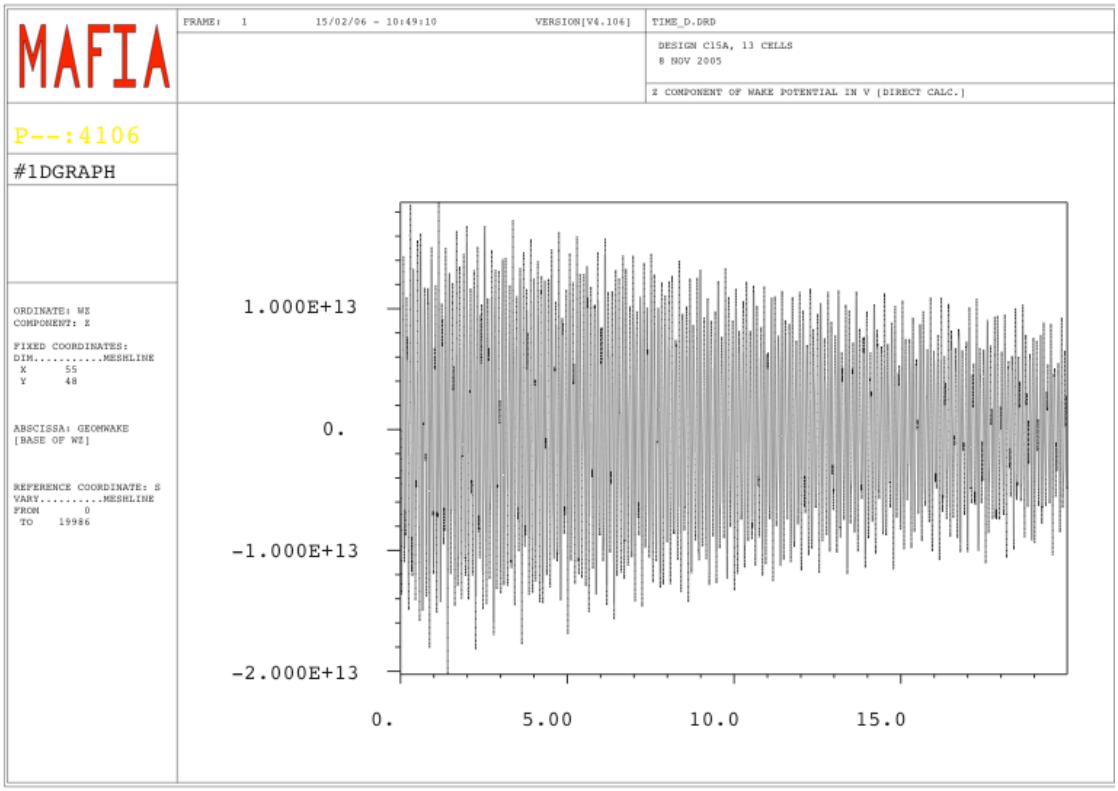

Figure 8. $W_z(s)$ for 20ps bunch, run 7.5mm off axis in the $+x$ direction for 20m.

Figure 9 shows the Fourier transform of the result for a 6m run, with the bunch directly on axis, so as to excite only the monopole modes. The plotted quantity is power, *i.e.* the sum of the magnitudes of the positive and negative frequency components. The conventions for the discrete transform are given in the second appendix. The phase of the Fourier transform shows no modal structure above 30GHz, as makes sense from the width of the exciting pulse. Above 30 GHz, the phase follows the straight line $\pi(0.003194f - 0.478814)$ radians, with the frequency in GHz. Figure 10 is the same as figure 9, but on a different scale. We see modes at 2.80, 6.06, 7.16, 9.31, 10.82 and 12.17GHz. These correspond to the first six intersections from the light cone analysis, and were all found in the frequency domain analysis. On the linear scale, it is clear that nearly all the wakefield power is in the long-lived modes, and the 2.80 TM_{010} and 7.16 hybrid modes. Curiously, the eigenfinder value for the frequency of the 12.17GHz mode is more than the 50MHz resolution below the time domain prediction. However, if there are any other high $R^{(n)}/Q$ modes in this region, they have eluded detection.

The next step was to run the exciting bunch and the trailing bunch through the cavity off axis 7.5mm in the $+x$ and $+y$ directions. This excites both dipole and quadrupole modes. The Fourier transform, with the transform of the on axis case

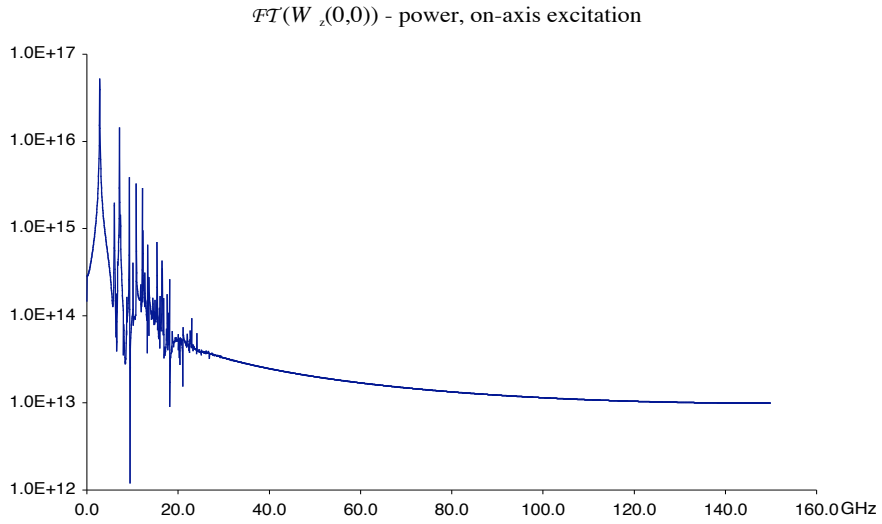

Figure 9. The Fourier transform of the longitudinal wakefield evaluated on-axis, for exciting bunch on-axis.

The next step was to run the exciting bunch and the trailing bunch through the cavity off axis 7.5mm in the $+x$ and $+y$ directions. This excites both dipole and quadrupole modes. The Fourier transform, with the transform of the on axis case subtracted out, is in figure 11. Both the $+x$ and $+y$ results are shown; they are substantially identical.

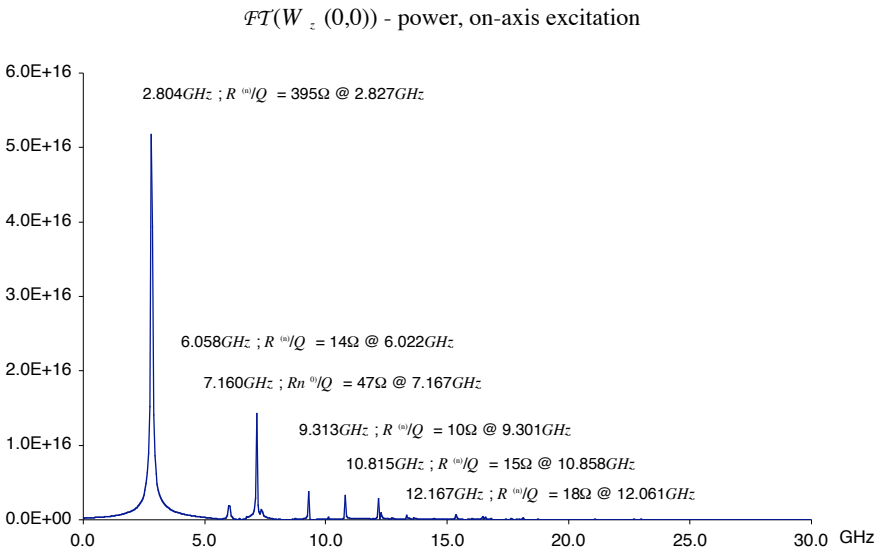

Figure 10. Same as figure 9. The $R^{(n)}/Q$ values and frequencies from the eigenfinder are marked.

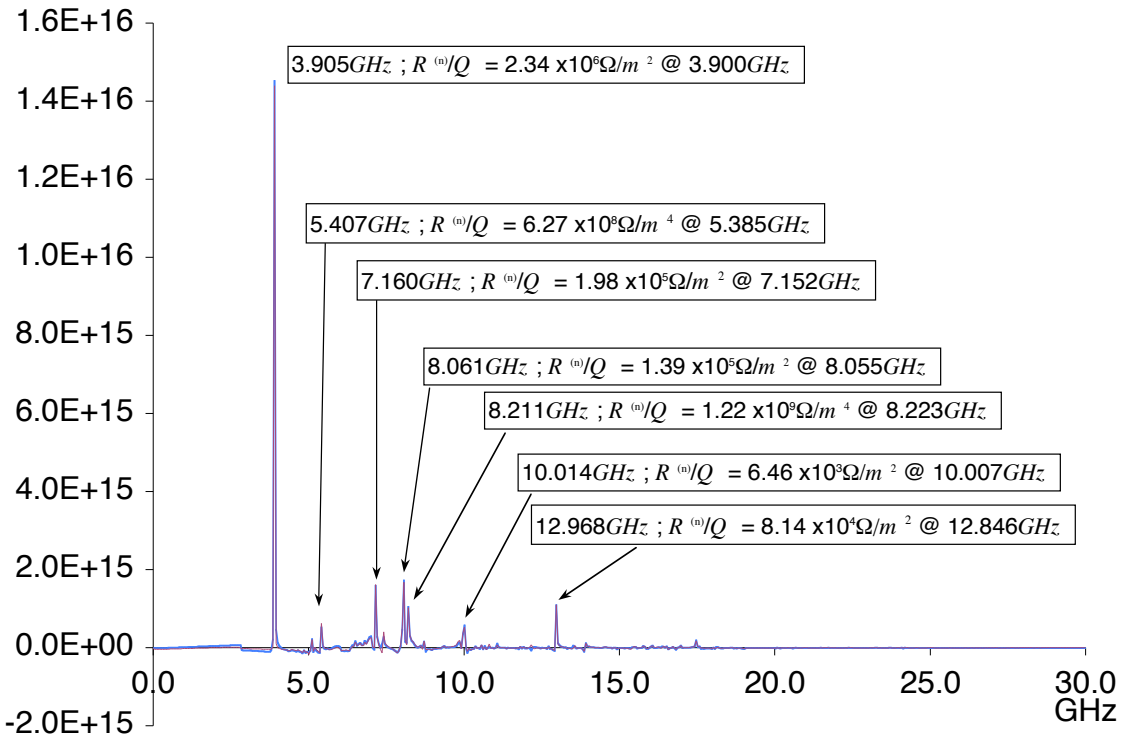

Figure 11. The Fourier transform of the longitudinal wakefield 7.5mm off-axis, with the on-axis spectrum subtracted.

We see peaks from the 3.9GHz dipole, as well as dipoles at 7.15, 8.06, 10.01, and 12.97GHz. These bands were all found in the periodic mode analysis. The 12.97GHz mode motivated running the eigenfinder up to 13GHz for dipole modes. Again, we note that the frequency given by the eigenfinder is below the one from the time domain, by abut twice the 50MHz resolution. A search up to m = 4 has failed to find any other candidates. At 13GHz, the 1mm mesh in the time domain analysis corresponds to ~λ/25, but a detailed understanding of how this would systematically bias frequency numbers down is not on hand. There are quadrupoles at 5.41 and 8.21GHz, also found in the periodic mode analysis, and possibly a mode at 17.47GHz. Note however the much different scale of figure 11 in comparison to figure 10; many of the smaller features in figure could be computational artifacts. Also, 7.5mm is a much larger offset that we expect in any application.
The scales of figures 9 through 11 may be understood better by taking the value 204keV/mm from equation 8, and multiplying it by (7.5mm) $sin(2\pi$ 3.9GHz $t)$ to obtain a quantity that is basically like the longitudinal wakefield, but is due to the klystron rather than proceeding bunches. Feeding this pseudo-wakefield through this same Fourier transform code yields a power peak at 3.9GHz that is $(9.48 \times 10^4 \text{ V})^2$. The peak in figure 11 is $(1.20 \times 10^8 \text{ V/C})^2$ and so for a single 10nC bunch, the TM_{110} π wake field is $(10\text{nC} \bullet 1.20 \times 10^8 \text{ V/C}) / (9.48 \times 10^4 \text{ V}) = 10^{4.9}$ times smaller than the klystron field.

We may now decide what modes should be considered important. We would like to get the energy loss and angular deflection correct to within a few percent. From equation 6 and the expression for energy loss, we see that the relevant quantities are $R^{(n)}/Q$ ($\omega_n r^{2m}$) – essentially, the loss parameters that will be discussed below. From equation 7 and the expression for angular deflection, the relevant figure of merit is $R^{(n)}/Q$ ($m r^{2m-1}$). For the "Major modes only" option, modes are included if either figure of merit was more than 3% of its maximum over all the modes with a beam 5mm off-axis; setting the cut below this level sharply increased the number of included modes. The figure of merit K = $Log_{10}(0.5*(f_M+f_E) / |f_M-f_E|$ where $f_{M,E}$ are the frequencies from the eigenfinder was also studied, along with a similarly value using the $R^{(n)}/Q$ values. In the end the only requirement used is that the simulated bead pulls allowed that both EE and BB boundary solutions could be found. Cases where this was not true always had large amounts of beampipe energy.

This selects all the modes identified in figures 10 & 11, plus a few. In some cases, 2 or 3 adjacent modes in the same passband contribute; in others, modes which have a high transverse wake relative to their longitudinal wake appear in the sum. There are a total of 21 major modes, not counting the degeneracy in the multipole modes. For the ILC beam parameters, the same modes were selected despite the smaller overall offset of the beam. This is because the

contribution of a multipole term is compared to the contribution of the largest multipole term, smaller though that might be in absolute terms.

Short range wakes and the 2-d time domain analysis

The second way in which the time domain studies were used to support the frequency domain analysis was to evaluate the broadband loss parameter. In addition to the energy left in the various eigenmodes of the cavity by the passing bunch, there will also be, for such short bunches, energy lost to the continuum spectrum up to a frequency determined by the bunch length.

Writing the linear charge density

$$\lambda(s) = \frac{1}{\sqrt{2\pi}\sigma}\exp\left(\frac{-(s-s_0)^2}{2\sigma^2}\right),$$

the energy lost by a bunch as it passes through the cavity is

9) $$\Delta E = q^2 k_{tot}(\vec{r}) = q^2 \int_{-\infty}^{+\infty} ds\, \lambda(s) W_{//}^{FEM}(\vec{r}, s)$$

where $W_{//}^{FEM}(\vec{r}, s)$ is the quantity produced by the code. The total loss parameter $k_{tot}(\vec{r})$ is the sum of modal loss parameters

$$k^{(n)}(\vec{r}) = \frac{\omega_n}{2}\frac{R^{(n)}}{Q} r^{2m}\cos^2\left[m(\phi - \phi_n)\right] = \frac{\left\{V_n(\vec{r})\right\}^2}{4U_n}$$

and an additional term from non-resonant broadband effects. Details are banished to the third appendix.

Figure 12 shows the wakefield, both on and off axis, and the bunch profile, for a 20ps bunch. The integration of equation 9 was done with the Newton-Cotes formula with error $\mathcal{O}[\Delta x^4]$, and the result was the same, to the reported significance, as the result from the formula of order $\mathcal{O}[\Delta x^3]$. Figure 13 shows $k_{tot}(\vec{r} = \vec{0})$ for several bunch lengths, using both the “direct” and “indirect”

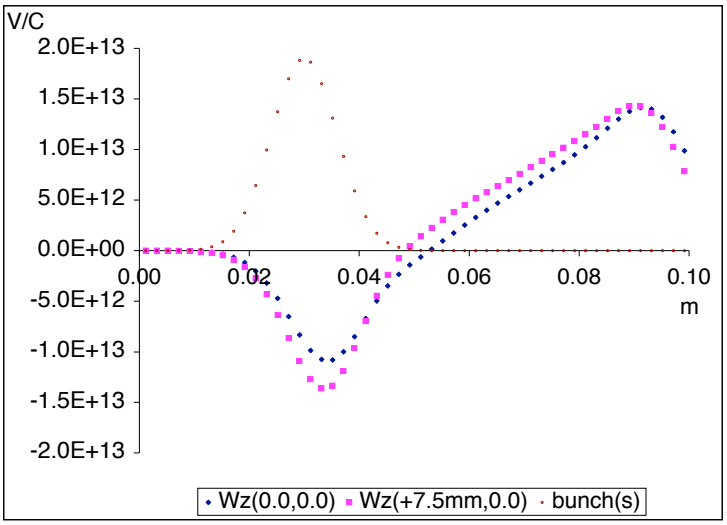

Figure 12. Short-range wakefield W_z and bunch profile.

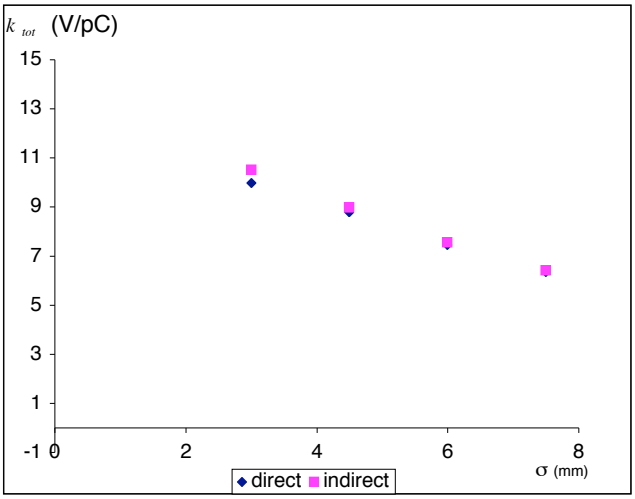

Figure 13. k_{tot} for on-axis beam, using both direct and indirect integration, for a range of Gaussian bunch lengths.

integration options. For the "indirect" option, a washer with 28mm ID was put at each end of the beampipe.

Considering only the important modes described above, and weighting them with $exp(-(\omega\sigma_t)^2 / 2)$ to allow for the finite width of the exciting Gaussian bunch (see the third appendix), the sum of modal loss factors is 8.5V/pC, in reasonable agreement with the values in figure 13. The sum of the modal loss factors from

the three largest contributors out of the TM_{010} band is 6.3V/pC, and contributions from the multipole modes are small – on the order of 0.1V/pC, typically.

Figure 13 gives a reasonable estimate of the loss parameter down to a bunch length of 3mm, but we are interested in applications with bunch lengths of 0.3mm. To understand effects on this scale, a 2-d model with 75μm mesh was constructed. Even this however was insufficient to provide accurate simulations of the needed bunch lengths.

Analytic techniques[9] permit the calculation of short range wakes, with some approximations. The short range wake is taken to be determined by the iris radius, spacing, and thickness; details of the rounding on the iris and the shape of the cavity cells near the equator are neglected. For longitudinal wakes, only monopole terms are counted; only dipole terms are included in the expansions for transverse fields. Forms exist for single-cell and infinite periodic structures; the intermediate case of a multi-cell cavity lies somewhere between. A common approach to these shortcomings[10] is to generalize the analytic forms, typically replacing physical cavity dimensions with arbitrary constants, and fitting the

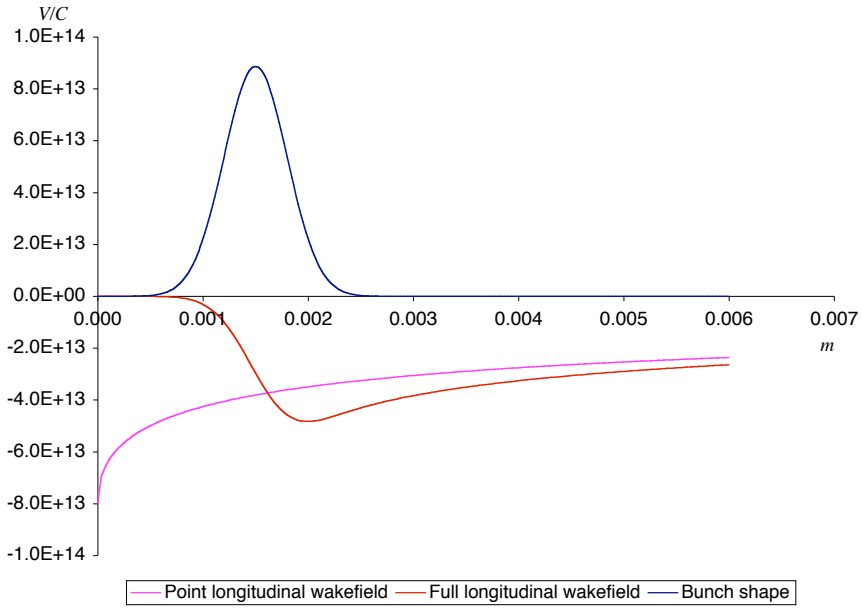

Figure 14. Analytic evaluation of the longitudinal wakefield.

[9] R.L. Gluckstern, Phys. Rev. D, **39**, (1989) 2773, 2780; A.V. Fedotov, R.L. Gluckstern, and M. Venturi, Phys. Rev. ST-Accelerators and Beams, **2**, (1999) 064401; K. Yokoya and K.L.F. Bane, in *Proceedings of the 1999 IEEE Particle Accelerator Conference, New York, N.Y.* (Piscataway, NJ, 1999) p. 1725; see also K.L.F. Bane SLAC-PUB-9663.
[10] *See e.g.*, T.Weiland and I. Zagorodnov, TESLA Report 2003-19 and I. Zagorodnov, T Weiland and M. Dohlus, TESLA Report 2004-01.

resulting forms to computational results. Here, we use the analytic results to identify when computational results become invalid as the bunch length approaches the mesh size. A comparison of the numeric and analytic loss parameters permits a reasonable estimate of the values for short bunch lengths.

Figure 14 shows the analytic form of the longitudinal wakefield for a point charge, $W_{//}(s) \approx A_{//} \exp(B_{//} s)\, erfc\left(\sqrt{B_{//} s}\right)$, where $A_{//} = NLZ_0 c/\pi a^2$, $B_{//} = \pi/4 s_{00}$, and s_{00} = 1.683mm for our geometry. Figure 14 also shows a 1ps Gaussian charge distribution and the resulting convolution.

Figure 15 plots the analytic form of the transverse wakefield, $W_{\perp}(s) = A_{\perp}\, r \left[1 - \left(1 + \sqrt{s/s_{00}}\right)\exp\left(-\sqrt{s/s_{00}}\right)\right]$, where $A_{\perp} = 4NLZ_0 c s_{00} / \pi a^4$, and again, the corresponding convolution with a Gaussian spot. The fields are evaluated with offset r = 1.05mm, corresponding to a mesh line on the MAFIA model. Also shown on figure 15 is the transverse deflecting field of a single 13 cell cavity operated at 6MV/m. The transverse wakes are small with respect to the deflecting field; were this not the case, the cavity would be creating banana-shaped bunches, a very bad outcome for the ILC application in particular.

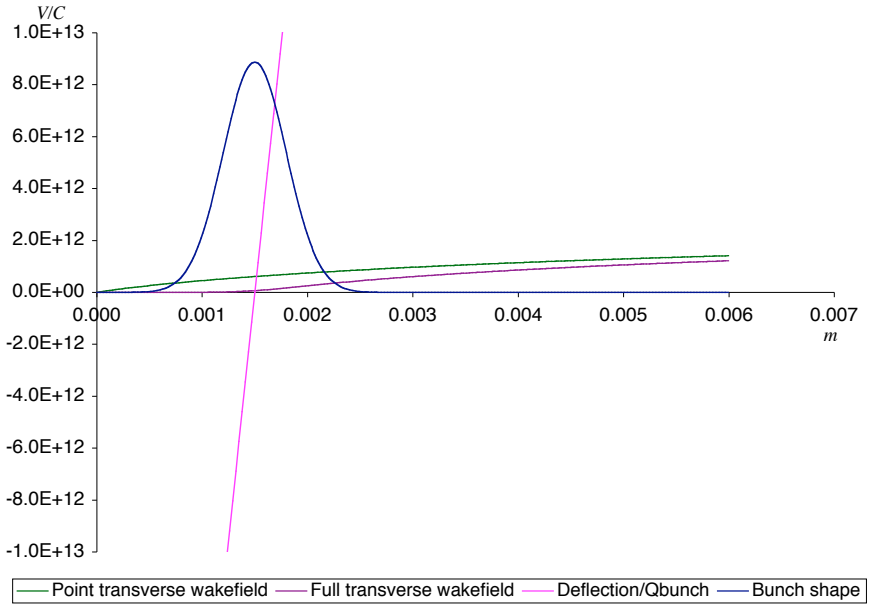

Figure 15. Analytic evaluation of the transverse wakefield at r = 1.05mm.

In the MAFIA 2-d time domain package, “open” boundary conditions were used and, and the “zoom” option was set to 4. For longitudinal wakefields, the azimuthal flag must be set to 0 and the desired answer is in the data bank for the

"wz" field; for the transverse wakes, these are 1 and "wr", respectively. Transverse fields were again evaluated at 1.05mm offset. With these settings, the computed wakefields began to deviate from the expected results at about 4 or 5ps bunch lengths. Below this, non-physical bumps, as shown in figure 16 for a 2ps bunch evaluation of transverse wakes, appeared.

Figure 17 shows the analytic and computed values loss parameter k_{tot} as a function of bunch length, with the data of figure 13 also included. At 1ps, the total loss parameter is 28.1V/pC analytically; the numeric results extrapolate out to about 25V/pC. For trains with 3000 bunches of 3.2nC at a 5Hz repetition rate, this corresponds to about 8.6W/m of active cavity. This neglects losses at narrow apertures such as gate valves immediately upstream of the cavity in the beamline. Of this 8.6W/m, 2.6W/m will be in the identified trapped modes; it and a (probably small) fraction of the remaining 6W/m will be dissipated as cryogenic load. The balance will be radiated out the beampipes as a broadband spectrum going up to the THz scale. Similar effects have led DESY to insert ferrite dampers in their cryomodules

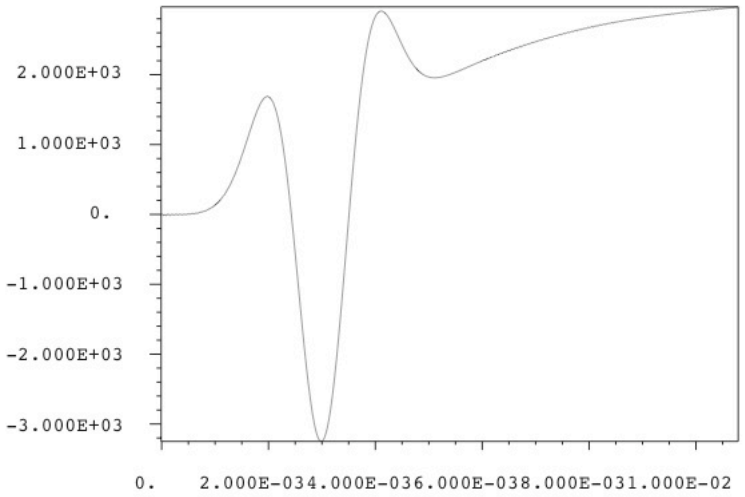

Figure 16. Example of non-physical MAFIA result for transverse wakefield.

Figure 18 shows the corresponding quantity for the transverse wakefield, $k_{\perp\, tot}(\vec{r}) = \int_{-\infty}^{+\infty} ds\, \lambda(s) W_{\perp}^{FEM}(\vec{r}, s)$ at 1mm beam offset; effectively then the units on the vertical axis are V/pC-mm. At 1ps, the analytic result is 0.085 V/ pC-mm, and the extrapolation of the numeric results would come out about 25% lower.

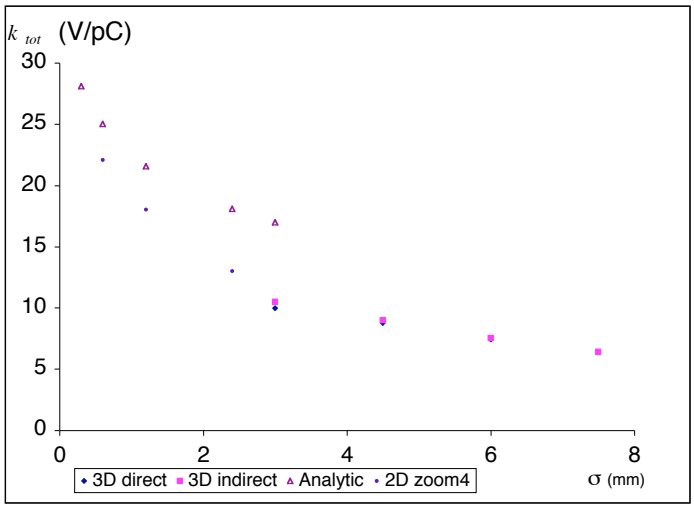

Figure 17. Longitudinal loss parameter for short bunch lengths.

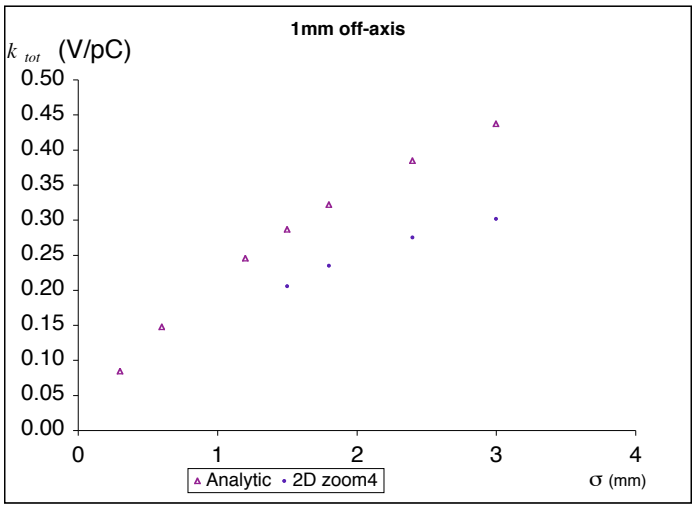

Figure 18. Transverse loss parameter for short bunch lengths at 1mm offset.

.

Results and conclusions

The wakefields in a 13 cell the 3.9GHz deflecting mode cavity with ideal geometry have been modeled in both the time domain and frequency domain. The former serves as a check on the latter. While values of Q_{EXT} to be plugged in to the frequency domain calculation are still nominal numbers, new ones can be readily inserted. Losses onto the surface of the cavity when it sits at 4.15K may be included, but are small.

The important modes are listed in table 4. The total longitudinal loss parameter is 28 V/pC for 1ps bunches. For a pure δ-function bunch, the loss parameters total about 6.3V/pC are from the three TM_{010}modes. The monopole modes altogether contribute about 11.3V/pC and the dipole modes contribute on the order of 0.1V/pC or less for a 1mm off-axis beam.

m	f (MHz)	$R^{(\mathrm{m})} / Q$ (Ω/m^{2m})	G
0	2822.83	186.9	178.2
0	2827.38	395.4	178.2
0	2831.04	127.8	178.3
0	5994.83	7.1	454.5
0	6022.36	14.1	456.2
0	7152.77	30.8	345.5
0	7166.88	46.7	340.8
0	7175.79	9.6	337.7
0	9301.33	10.0	556.7
0	9310.83	6.5	526.4
0	10848.05	5.2	547.9
0	10858.40	15.0	528.3
0	10865.89	6.3	514.8
0	12055.49	15.6	714.2
0	12060.67	18.0	711.9
1	3900.00	2339141	225.2
1	7103.81	133968	446.4
1	7152.26	198325	421.1
1	8054.68	138620	517.3
1	12846.07	81460	1038.5

Table 4. The major modes for the 13 cell cavity.

Figure 19 shows the resulting changes in energy and bunch direction for the NewMuon/SMTF beam parameter set, for a given, nominal yet reasonable set of Q_{EXT} values. For the three important TM_{010} modes, Q_{EXT} was taken to be 1.3 x10^5; for the powered mode, 1.5 x10^7; for the other-polarization TM_{110} mode and all higher order modes, 1.0 x10^6. The beam position is 0.8mm in x (the deflection plane) and 0.6mm in y, and the bunch is 1ps long; the cavity is taken to be operated at 6MV/m field strength.

The notable conclusions are that the short-range energy loss calculated from k_{tot} is only a bit larger than the long-range losses, and both are about three orders of magnitude below the beam energy. For the beam off-axis as shown, the longitudinal component of the 3.9GHz mode couples strongly to and removes power from the bunch train. There is a smearing of the center of the spot, bunch-to-bunch that will appear as a loss of beam-slice resolution from long-range wakes, but this is on the order of a few tens of μrad, and the deflection from the driven mode to create the beam slice is 1.83mrad.

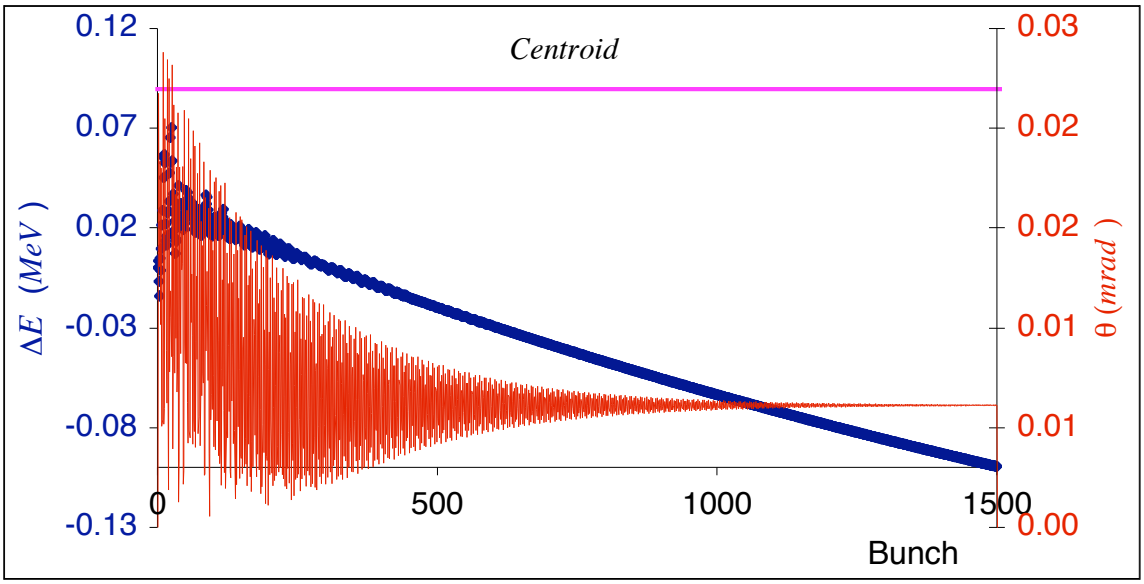

Figure 19. Predicted change in energy and deflection angle of bunch centers, vs. bunch number, for the NewMuon/SMTF beamline.

Figure 20 shows the deflection angle of the head of the bunch ($1\sigma_z$ ahead of the bunch center) minus the deflection at the center of the bunch. A large effect appears in the x direction. What is happening is that 1500 bunches of 3.2nC, losing each an energy as shown in figure 19, have left something like 200mJ of wakefield energy in the 3.9GHz mode. That corresponds to about 70% of the driven deflection field. This field modulation must be either addressed

dynamically through the LLRF system, or we will need to have very good beam-to-cavity alignment.

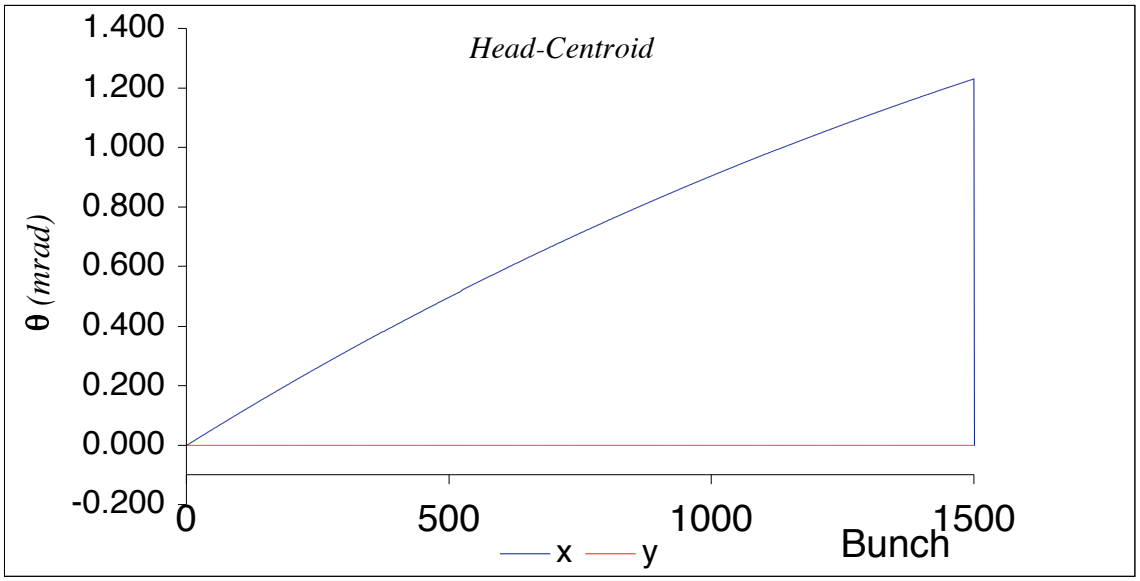

Figure 20. Predicted crabbing angle vs. bunch number for the NewMuon/SMTF beamline.

The other-polarization TM_{110} mode is not quite as serious a problem, due to the difference between its frequency and the resonances of the beam structure. Indeed the above results are still broadly obtained if the values of Q_{EXT} are multiplied by 100 for the other-polarization and higher order modes. Encouraging results occur if we imagine that that both the HOM and LOM couplers actually have Q_{EXT} values 1000 times worse than those used here.

If the values of Q_{EXT} for the TM_{010} modes are increased by two orders of magnitude, the contributions to changes in bunch energy from these monopole modes becomes important, as shown in figure 21. The interference of the three important modes in this passband is evident.

Synchronization of the beam structure with the cavity frequency is however crucial. If the 3.9GHz π TM_{110} mode is shifted up by 100Hz for example, an angular deflection of 7mrad in the x direction of the bunch centers will occur in the first 1500 bunches.

Figures 22 and 23 show the resulting changes in energy and bunch direction for the ILC beam parameter set. Here, the beam enters 520nm off axis, in the direction of the deflection. The real distance off axis might be several times this value. Bear in mind that here we are still simulating a single 13-cell cavity, which

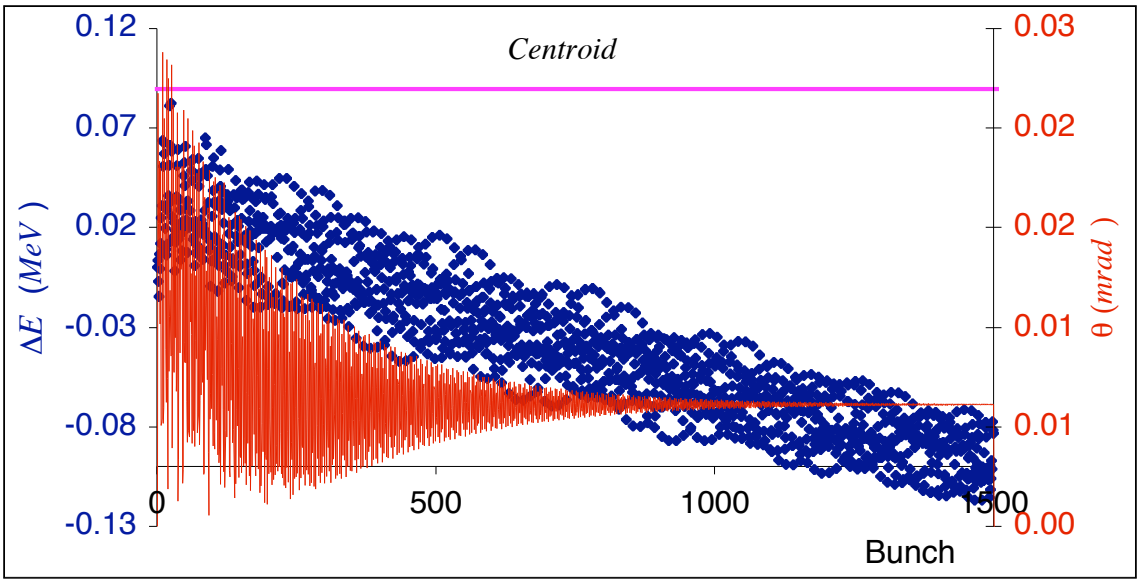

Figure 21. Similar to figure 19, but with Q_{EXT} of 1.3 x10^7 for the TM_{010} band.

is not the baseline proposal. The values of Q_{EXT} are the same as for the NewMuon/SMTF parameter set, except that a value of 5 x10^5 was used for the π TM_{1210} band.

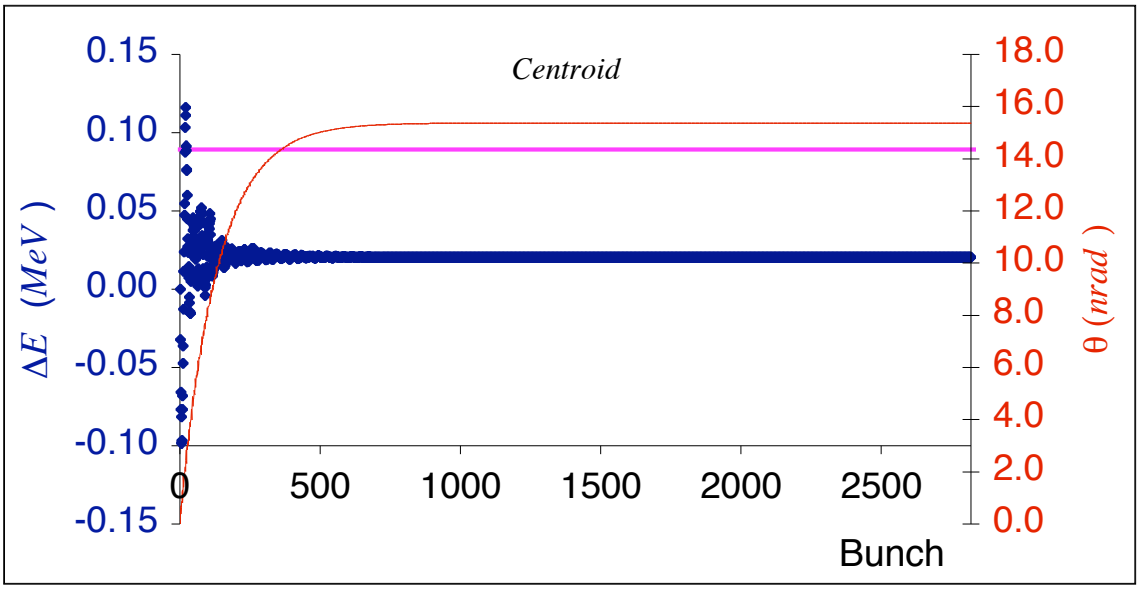

Figure 22. Predicted change in energy and deflection angle of bunch centers, vs. bunch number, for a single 13-cell cavity in the ILC beamline.

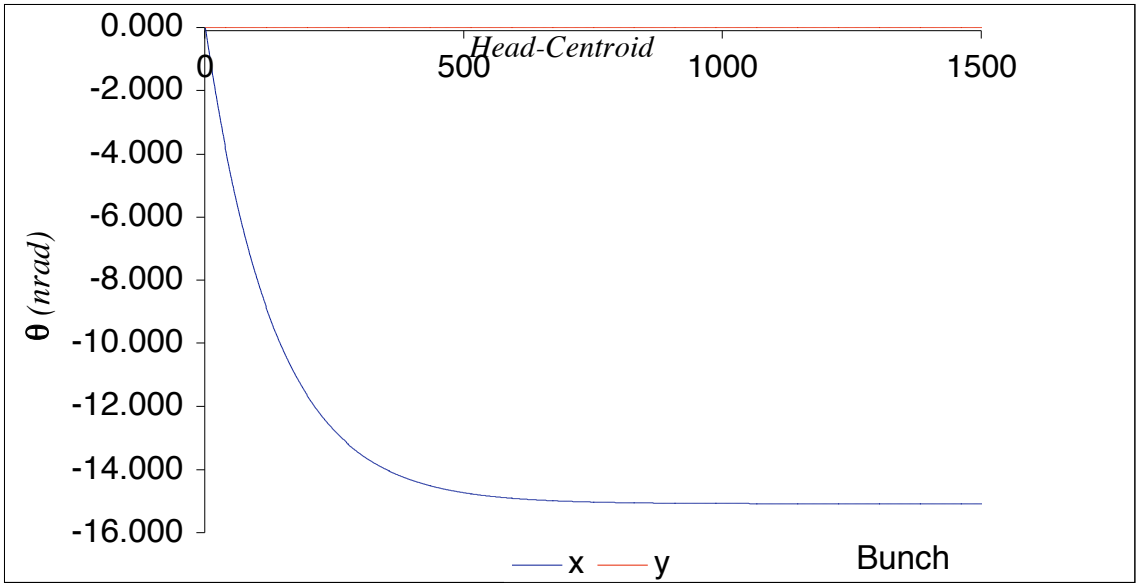

Figure 23. Predicted crabbing angle vs. bunch number for a single 13-cell in the ILC beamline.

A careful study of manufacturing imperfections has not been made, and this is the worst approximation in the analysis presented here. In particular, the case where a HOM or LOM lands on a multiple of the bunch spacing will change the behavior of the system wildly. Not in the least, it will dramatically increase the power load through the coupler systems. Work by S. Tariq and T.Khabiboulline shows that for power levels as low as 4W (after duty factor) one will need coax cables with IDs of 1.8mm or more to prevent thermal runaway.

A less serious approximation, although one that should still be examined, is the assumption that the 7.1, 8.0 and 12.8GHz dipole bands are indeed pinned to the cavity asymmetries and are not determined by the beam orientation.

There is a large parameter space. In addition to variations in frequency, R/Q values, and electrical centers due to manufacturing imperfections, values of Q_{EXT} are still nominal. As of this writing, in fact we are finding that the design of couplers with adequate mechanical strength and reasonable tuning sensitivity is more difficult than anticipated.

There remains a need to understand the surface currents on the coupler tips, particularly for the LOM coupler. However, unlike the case of the main cavity walls, the heat flow problem is not very easy to solve, particularly in light of well known sample-to-sample variations in R_{SURF} and thermal conductivities for niobium.

Finally, for the ILC application, we should recall that TESLA discovered that one could trap modes in multi-cavity strings that were not trapped in a single-cavity case.

Acknowledgements

We would like to thank Valeri Lebedev, Phillipe Goudket, Helen Edwards, John Corlett, Jacek Sekutowicz, Nikolay Solyak, Timergali Khabiboulline, Ivan Gonin, and particularly Rainer Wanzenberg for many helpful conversations.

The first appendix

The following derivation follows closely that of Wanzenberg and Weiland[11]. What is different here is that the assumption of azimuthal symmetry is dropped. The basic procedure, probably originally due to Condon[12], is to:

a. Expand the magnetic potential $\vec{A}$ into a set of orthogonal functions that are the eigenfunctions for the infinite-conductivity limit of the empty cavity (*i.e.*, sans beam).
b. Write the magnetic potential, the beam current, and ultimately the electric field, in the frequency domain.
c. Write the wake potential in terms of the frequency domain electric field and simplify it.

This will give equation (1). Equations (2) through (4) will be shown subsequently.

To find the set of orthogonal functions that are the eigenfunctions for the infinite-conductivity limit of the empty cavity, note that when $\vec{J} = 0$, the vector potential satisfies the wave equation $\left\{\nabla^2 - {}^{1}\!/_{c^2}\,\frac{\partial^2}{\partial t^2}\right\}\vec{A} = 0$, which responds well to the method of separation of variables. So each of the n solutions are $\vec{A}_n(\vec{r},z,t) = \vec{a}_n(\vec{r},z)e^{i\omega_n t}$, with the convention that ω_n may take negative values, making it unnecessary to write $e^{-i\omega_n t}$ solutions explicitly. In the frequency domain the wave equation is just $\nabla^2\vec{a}(\vec{r},z) = -\left({}^{\omega^2}\!/_{c^2}\right)\vec{a}(\vec{r},z)$.

In any expansion, there must be some orthonormality condition. In this case the energy stored in the cavity for a given mode provides the normalization constant. For any specific mode n with a corresponding given field level, the energy in the cavity is

$$U_n = \frac{\varepsilon_0}{2}\iiint_{cavity\ volume} d^2\vec{r}\,dz\left\{\vec{E}_n^*(\vec{r},z,t)\bullet\vec{E}_n(\vec{r},z,t)\right\}_{t=t_0}$$

where $t = t_0$ means that the electric field for that mode is to be evaluated at the time when the magnetic field (which is 90° out of phase) is zero. Each eigensolution may also be scaled by some arbitrary constant, thereby changing U_n, but here we just assert that some particular scaling has been chosen and do not have to belabor the issue further. Then the normalization is

---

[11] T.Weiland, R.Wanzenberg, in "Frontiers of Particle Beams: Intensity Limitations", the joint US-CERN Particle Accelerator School, Hilton Head S.C. U.S.A., 1990; and R.Wanzenberg, TESLA note 2001-33. See also appendix A of FNAL TM 2144.
[12] E.U.Condon, J.Appl.Phys. **12** (1941) 129.

$$U_n = \frac{\varepsilon_0}{2}\iiint_{cavity} d^2\vec{r}\,dz\left\{\vec{E}_n^*(\vec{r},z,t)\bullet\vec{E}_n(\vec{r},z,t)\right\}_{t=t_0}$$

$$= \frac{\varepsilon_0}{2}\iiint_{cavity} d^2\vec{r}\,dz\left\{-\frac{\partial}{\partial t}\left[\vec{a}_n(\vec{r},z)e^{i\omega_n t}\right]\right\}^*\bullet\left\{-\frac{\partial}{\partial t}\left[\vec{a}_n(\vec{r},z)e^{i\omega_n t}\right]\right\}_{t=t_0}$$

$$= \frac{\varepsilon_0}{2}\omega_n^2\iiint_{cavity} d^2\vec{r}\,dz\;\vec{a}_n^*(\vec{r},z)\bullet\vec{a}_n(\vec{r},z).$$

Next, expand the vector potential in these modes. If we allow the coefficients of the expansion $\alpha_n(t)$ to depend on time, it will be possible to allow for phenomena such as ring-down caused by external couplers:

$$\vec{A}(\vec{r},z,t) = \sum_n \alpha_n(t)\,\vec{a}_n(\vec{r},z)\,e^{i\omega_n t}.$$

This being the first time we expand in modes, it is worth belaboring what the sum over n includes. It includes in principle a full set of eigenfunctions up to infinite frequency; that would be both a discrete spectrum at lower frequencies (f < a few times c/ρ, where ρ is the size of the largest aperture of the structure) and a continuum at higher frequencies. There is also the possibility of a nearly discrete spectrum at higher frequencies that have a relatively narrow width because the spatial characteristics of the mode prevent its rapid dissipation out through the cavity apertures. These "trapped modes" and high frequency continuum are ignored in this treatment. Their effects can be understood with time domain modeling. The sum over n includes cases of frequency degeneracy. In particular, for a pillbox-like cavity, there will be two dipole modes of each type. In a real cavity, manufacturing asymmetries will give them slightly different frequencies; in the cavity studied here, an intentional azimuthal asymmetry separates the modes by some 10MHz. Both modes are included in the sum. Similarly, quadrupole modes have a two-fold degeneracy. Unlike the situation when we take the Fourier transform of quantities such as the beam's time structure, we do not have to include modes of negative frequencies. Here we are generalizing the real field quantity denoted by $\vec{A}$ into a complex quantity cleverly denoted by $\vec{A}$, with the intent of later taking the real part. For real numbers a and b, the real part of $ae^{i\omega t} + be^{-i\omega t}$ is the real part of $(a+b)e^{i\omega t}$, and so we may get by with only positive frequencies.

Insert the expansion into the inhomogeneous Maxwell equation for $\vec{A}$ (neglecting the space charge term $\nabla\Phi$) and then apply the frequency domain wave equation for each particular $\vec{a}_n(\vec{r},z)$:

$$\frac{1}{\varepsilon_0}\vec{J}(\vec{r},z,t) = \sum_n\left[\omega_n^2 + \frac{\partial^2}{\partial t^2}\right]\left(\alpha_n(t)e^{i\omega_n t}\,\vec{a}_n(\vec{r},z)\right).$$

Apply the orthonormality condition

$$\frac{1}{\varepsilon_0}\iiint_{cavity} d^2\vec{r}\,dz\;\vec{a}_n^{*}(\vec{r},z)\bullet\vec{J}(\vec{r},z,t) = \iiint_{cavity} d^2\vec{r}\,dz\;\vec{a}_n^{*}(\vec{r},z)\bullet\sum_{n'}\left[\omega_{n'}^2+\frac{\partial^2}{\partial t^2}\right]\left(\alpha_{n'}(t)e^{i\omega_{n'}t}\;\vec{a}_{n'}(\vec{r},z)\right)$$

$$= \sum_{n'}\left[\omega_{n'}^2+\frac{\partial^2}{\partial t^2}\right]\alpha_{n'}(t)e^{i\omega_{n'}t}\iiint_{cavity} d^2\vec{r}\,dz\;\vec{a}_n^{*}(\vec{r},z)\bullet\vec{a}_{n'}(\vec{r},z)$$

$$= \sum_{n'}\left[\omega_{n'}^2+\frac{\partial^2}{\partial t^2}\right]\alpha_{n'}(t)e^{i\omega_{n'}t}\,\delta_{n'n}\frac{2U_{n'}}{\varepsilon_0\omega_{n'}^2}$$

$$= \frac{2U_n}{\varepsilon_0\omega_n^2}\sum_{n}\left[\omega_n^2+\frac{\partial^2}{\partial t^2}\right]\left(\alpha_n(t)e^{i\omega_n t}\right)$$

and use the Fourier transform (conventions in the second appendix). Since $\mathcal{F}[\frac{\partial^r}{\partial t^r}f(t)] = (i\omega)^r\mathcal{F}[f(t)]$ and $\mathcal{F}[e^{i\omega_n t}f(t)] = \tilde{f}(\omega-\omega_n)$, the Fourier transform of $\alpha_n(t)\,e^{i\omega_n t}$ is given by

$$\tilde{\alpha}_n(\omega-\omega_n) = \frac{1}{2U_n}\left(\frac{\omega_n^2}{\omega_n^2-\omega^2}\right)\iiint_{cavity} d^2\vec{r}\,dz\;\;\vec{a}_n^{*}(\vec{r},z)\bullet\tilde{J}(\vec{r},z,\omega)$$

where $\tilde{J}(\vec{r},z,\omega)$ is a vector quantity, the current density after a Fourier transform in the time but not the spatial coordinates. The similarly transformed vector potential is $\tilde{A}(\vec{r},z,\omega) = \sum_n \tilde{\alpha}_n(\omega-\omega_n)\,\vec{a}_n(\vec{r},z)$. The beam current produced by the exciting beam is $\vec{J} = c\,q_1\,\delta(z-ct)\delta^2(\vec{r}-\vec{r}_1)\hat{z}$, which has Fourier transform $\tilde{J}(\vec{r},z,\omega) = q_1 e^{-i\omega z/c}\,\delta^2(\vec{r}-\vec{r}_1)\hat{z}$. Now we can write the electric field in the excited cavity in the frequency domain:

$$\tilde{E}(\vec{r},z,\omega) = -(i\omega)\tilde{A}(\vec{r},z,\omega)$$

$$= -i\omega\sum_n \tilde{\alpha}_n(\omega-\omega_n)\,\vec{a}_n(\vec{r},z)$$

$$= \sum_n\left(\frac{-i\omega}{2U_n}\right)\left(\frac{\omega_n^2}{\omega_n^2-\omega^2}\right)\left[\iiint_{cavity} d^2\vec{\rho}\,d\xi\;\;\vec{a}_n^{*}(\vec{\rho},\xi)\bullet\tilde{J}(\vec{\rho},\xi,\omega)\right]\vec{a}_n(\vec{r},z)$$

$$= \left(\frac{-iq_1}{2}\right)\sum_n\left(\frac{\omega}{U_n}\right)\left(\frac{\omega_n^2}{\omega_n^2-\omega^2}\right)\left[\iiint_{cavity} d^2\vec{\rho}\,d\xi\;\;\vec{a}_n^{*}(\vec{\rho},\xi)\bullet\hat{z}\;\;e^{-i\omega\xi/c}\,\delta^2(\vec{\rho}-\vec{r}_1)\right]\vec{a}_n(\vec{r},z)$$

$$= \left(\frac{q_1}{2}\right)\sum_n\left(\frac{\vec{a}_n(\vec{r},z)}{U_n}\right)\left(\frac{\omega_n^2}{\omega^2-\omega_n^2}\right)\;\int_{-\infty}^{+\infty} d\xi\;\left[-i\omega\,\hat{z}\bullet\vec{a}_n(\vec{r}_1,\xi)\,e^{i\omega\xi/c}\right]^{*}$$

A similar expression for the magnetic field is not needed, because the Panofsky-Wenzel theorem, equation (4), lets us express all the desired quantities for the stiff beam case with just the z component of the electric field.

In the stiff beam approximation, $\hat{z} \bullet \left(\hat{z} \times \vec{B} \right) = 0$, so

$$W_{//}(\vec{r}_1, \vec{r}_2, s) = \frac{1}{q_1} \int_{-\infty}^{+\infty} dz \; E_z(\vec{r}_2, z, t = (s+z)/c)$$

$$= \frac{1}{q_1} \int_{-\infty}^{+\infty} dz \int_{-\infty}^{+\infty} \frac{d\omega}{2\pi} \, e^{i\omega t} \left(\frac{q_1}{2} \right) \sum_n \left(\frac{\hat{z} \bullet \vec{a}_n(\vec{r}_2, z)}{U_n} \right) \left(\frac{\omega_n^2}{\omega^2 - \omega_n^2} \right)$$

$$\int_{-\infty}^{+\infty} d\xi \; \left[-i\omega \, \hat{z} \bullet \vec{a}_n(\vec{r}_1, \xi) \, e^{i\omega \xi / c} \right]^*$$

$$= \frac{1}{4\pi} \sum_n {}^1\!/\!_{U_n} \int_{-\infty}^{+\infty} d\omega \, \frac{i\omega_n^2}{\omega(\omega^2 - \omega_n^2)} e^{i\omega s/c}$$

$$\int_{-\infty}^{+\infty} dz \left[-i\omega \, \hat{z} \bullet \vec{a}_n(\vec{r}_2, z) \, e^{i\omega z/c} \right] \int_{-\infty}^{+\infty} d\xi \; \left[-i\omega \, \hat{z} \bullet \vec{a}_n(\vec{r}_1, \xi) \, e^{i\omega \xi / c} \right]^*$$

Now let us do the integral over ω, the frequency spectrum of the beam. There are two poles, at $\pm\omega_n$. We'll do a loop in the complex ω plane, as shown in Figure A-1.

For $s >> 0$, a return path in the upper half-plane contributes negligibly to the integral; in this case, by causality the integrand must be non-zero. For $s << 0$, by causality the integrand must be zero, and this is satisfied by a return path is in the lower half-plane. For s within $\pm 2L$, the upper/lower assignment appears at first to depend on the sign of $s+z+\xi$, but actually does not. When the integrals

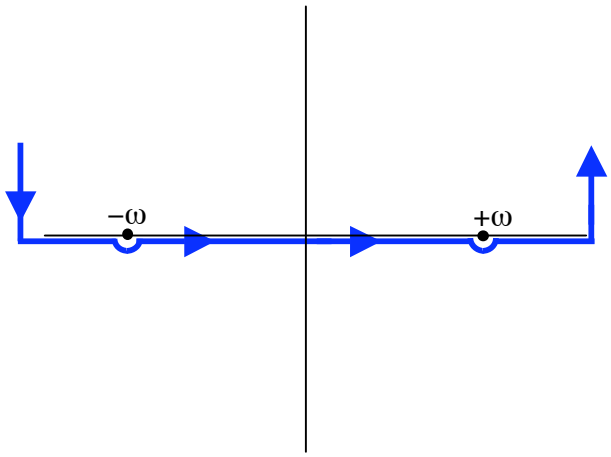

Figure A-1: The ω plane.

over z and ξ are done, they can not return quantities with factors like $e^{i\omega z/c}$ or $e^{i\omega\xi/c}$, as z and ξ have been integrated out. So we may take the upper half-plane for all $s > 0$, and similarly for $s < 0$.

For this contour, enclosing two first-order poles,

$$\int_{-\infty}^{+\infty} d\omega \, \frac{-i\omega\omega_n^2}{\left(\omega^2-\omega_n^2\right)} e^{i\omega s/c} \int_{-\infty}^{+\infty} dz \left[\hat{z}\bullet\vec{a}_n\left(\vec{r}_2,z\right)e^{i\omega z/c}\right] \int_{-\infty}^{+\infty} d\xi \left[\hat{z}\bullet\vec{a}_n\left(\vec{r}_1,\xi\right)e^{i\omega\xi/c}\right]^*$$
$$= 2\pi i\left[Rs\left(\omega=+\omega_n\right)+Rs\left(\omega=-\omega_n\right)\right]$$

and the residuals are

$$\left(\omega-\left\{\pm\omega_n\right\}\right)\left[\frac{-i\omega\omega_n^2}{\left(\omega^2-\omega_n^2\right)} e^{i\omega s/c} \int_{-\infty}^{+\infty} dz \left[\hat{z}\bullet\vec{a}_n\left(\vec{r}_2,z\right)e^{i\omega z/c}\right] \int_{-\infty}^{+\infty} d\xi \left[\hat{z}\bullet\vec{a}_n\left(\vec{r}_1,\xi\right)e^{i\omega\xi/c}\right]^*\right]_{\omega=\pm\omega_n}$$

and so the integral is

$$\pi\omega_n^2\left[\begin{array}{l} e^{i\omega_n s/c}\int_{-\infty}^{+\infty} dz \left[\hat{z}\bullet\vec{a}_n\left(\vec{r}_2,z\right)e^{i\omega_n z/c}\right] \int_{-\infty}^{+\infty} d\xi \left[\hat{z}\bullet\vec{a}_n\left(\vec{r}_1,\xi\right)e^{i\omega_n\xi/c}\right]^* \\ +e^{-i\omega_n s/c}\int_{-\infty}^{+\infty} dz \left[\hat{z}\bullet\vec{a}_n\left(\vec{r}_2,z\right)e^{-i\omega_n z/c}\right] \int_{-\infty}^{+\infty} d\xi \left[\hat{z}\bullet\vec{a}_n\left(\vec{r}_1,\xi\right)e^{-i\omega_n\xi/c}\right]^* \end{array}\right].$$

Shunt impedances, which conveniently describe the interaction of the cavity with the beam, are defined in terms of longitudinal integrals of the voltage:

$$V\left(\vec{r}\right)=\left|\int_{-L}^{+L} d\xi \; E_z\left(\vec{r},\xi,t=\xi/c\right)\right|.$$

This expression is phased, *i.e.* the origin of the ξ axis is implicitly selected to maximize the integral.

From $\vec{E}=-\partial\vec{A}/\partial t$, $\vec{E}\left(\vec{r},z,t\right)=-\left(i\omega_n\right)\vec{A}\left(\vec{r},z,t\right)$ in the time domain for any purely harmonic field of frequency ω_n, and so the last two integrals in the expression for $W_{//}$ resemble to $V\left(\vec{r}\right)$. Define $V_n\left(\vec{r}\right)\equiv\int_{-\infty}^{+\infty} d\xi\left[-i\omega_n\,\hat{z}\bullet\vec{a}_n\left(\vec{r},z\right)e^{i\omega_n\xi/c}\right]$ as the pure harmonic, single-mode complex generalization of $V\left(\vec{r}\right)$. As with all cases where complex-valued quantities are used to represent oscillating quantities, only the real part of $V_n\left(\vec{r}\right)$ is physical. Phasing so as to maximize the physical part requires that $V_n\left(\vec{r}\right)$ is in fact real. With this, the integral over ω becomes

$$\pi\left[\ e^{i\omega_n s/c}\ V_n(\vec{r}_2)\,V_n(\vec{r}_1)^* + e^{-i\omega_n s/c}\ V_n(\vec{r}_2)^*\,V_n(\vec{r}_1)\right] = 2\pi\,\cos(\omega_n s/c)\,V_n(\vec{r}_2)\,V_n(\vec{r}_1)$$

and the longitudinal wake field is just

$$W_{//}(\vec{r}_1,\vec{r}_2,s) = \frac{1}{2}\sum_n \cos(\omega_n s/c)\,\frac{V_n(\vec{r}_2)V_n(\vec{r}_1)}{U_n}.$$

Causality arguments do not provide a value for the wakefield at s = 0. However, the fundamental theorem of beam loading is that the self-wake, that is the energy lost by the exciting bunch, is one-half the wake directly behind the exciting bunch. For this reason, it is conventional to set

$$W_{//}(\vec{r}_1,\vec{r}_2,s=0) = \frac{1}{4}\sum_n \frac{V_n(\vec{r}_2)V_n(\vec{r}_1)}{U_n}.$$

Now for equation (2), which states that $W_{//}$ is a two-dimensionally harmonic function of both $\vec{r}_1$ and $\vec{r}_2$. Directly from the Maxwell equations,

$$\nabla^2\vec{E} - \frac{1}{c^2}\frac{\partial^2}{\partial t^2}\vec{E} = \frac{1}{\varepsilon_0}\left(\nabla\rho + \frac{1}{c^2}\frac{\partial}{\partial t}\vec{J}\right).$$

Quite apart from the no-space charge approximation, which is about the electric field produced by the bunch charge, the z component of the term on the right disappears for any beam traveling at velocity c:

$$\vec{J} = c\,\rho(\vec{r},\zeta = z - ct)\,\hat{z} \quad\Rightarrow\quad \frac{\partial}{\partial t}J_z = c\frac{\partial\rho}{\partial\zeta}\frac{\partial\zeta}{\partial t} = -c^2\frac{\partial\rho}{\partial\zeta} = -c^2\frac{\partial\rho}{\partial z}$$

leaving the wave equation

$$\nabla_\perp^2 E_z + \frac{\partial^2}{\partial z^2}E_z - \frac{1}{c^2}\frac{\partial^2}{\partial t^2}E_z = \frac{1}{\varepsilon_0}\left(\frac{\partial\rho}{\partial z} + \frac{1}{c^2}\frac{\partial}{\partial t}J_z\right) = 0.$$

This equation is valid at point 2, which is at some distance from the exciting charge. Introducing then the subscript 2,

$$\begin{aligned}\nabla_{\perp(2)}^2 W_{//}(\vec{r}_1,\vec{r}_2,s) &= \frac{1}{q_1}\int_{-\infty}^{+\infty} dz\ \nabla_{\perp(2)}^2 E_z\left(\vec{r}_2,z,t=(s+z)/c\right)\\ &= \frac{1}{q_1}\int_{-\infty}^{+\infty} dz \int_{-\infty}^{+\infty}\frac{d\omega}{2\pi}e^{i\omega t}\int_{-\infty}^{+\infty}\frac{dk}{2\pi}e^{-ikz}\ \nabla_{\perp(2)}^2\tilde{\tilde{E}}_z(\vec{r}_2,k,\omega)\Big|_{t=\frac{z+s}{c}}\end{aligned}$$

where $\tilde{\tilde{E}}_z$ is the z component of the electric field, Fourier transformed from both t to ω and from z to k. The advantage of using this quantity is that the wave equation in the doubly-transformed space is $\nabla^2_{\perp(2)}\tilde{\tilde{E}}_z + (-ik)^2\tilde{\tilde{E}}_z - \frac{1}{c^2}(i\omega)^2\tilde{\tilde{E}}_z = 0$, so

$$\begin{aligned}\nabla^2_{\perp(2)} W_{//}(\vec{r}_1,\vec{r}_2,s) &= \frac{1}{q_1}\int_{-\infty}^{+\infty} dz \int_{-\infty}^{+\infty}\frac{d\omega}{2\pi}e^{i\omega t}\int_{-\infty}^{+\infty}\frac{dk}{2\pi}e^{-ikz}\left(k^2 - \omega^2/c^2\right)\tilde{\tilde{E}}_z(\vec{r}_2,k,\omega)\Big|_{t=\frac{z+s}{c}} \\ &= \frac{1}{2\pi}\int_{-\infty}^{+\infty} dz\, e^{i\left(\omega z/c - kz\right)}\,\frac{1}{q_1}\int_{-\infty}^{+\infty} d\omega\, e^{i\omega s/c}\int_{-\infty}^{+\infty}\frac{dk}{2\pi}\left(k^2 - \omega^2/c^2\right)\tilde{\tilde{E}}_z(\vec{r}_2,k,\omega) \\ &= \delta\left(\omega/c - k\right)\frac{1}{q_1}\int_{-\infty}^{+\infty} d\omega\, e^{i\omega s/c}\int_{-\infty}^{+\infty}\frac{dk}{2\pi}\left(k^2 - \omega^2/c^2\right)\tilde{\tilde{E}}_z(\vec{r}_2,k,\omega) \\ &= 0.\end{aligned}$$

A symmetry argument that $\nabla^2_{\perp(2)} W_{//}(\vec{r}_1,\vec{r}_2,s) = 0$ implies $\nabla^2_{\perp(1)} W_{//}(\vec{r}_1,\vec{r}_2,s) = 0$, because of the explicit form of equation 1. In general, we should not expect a differential operator, D, to obey $D_{(1)} W_{//}(\vec{r}_1,\vec{r}_2,s) = D_{(2)} W_{//}(\vec{r}_1,\vec{r}_2,s)$; the former has terms like $\left[DV(\vec{r}=\vec{r}_1)\right]\cdot V(\vec{r}=\vec{r}_2)$ and the latter has terms like $\left[DV(\vec{r}=\vec{r}_2)\right]\cdot V(\vec{r}=\vec{r}_1)$ and both the derivatives and the value of V will be different at the two different evaluation points $\vec{r}_1$ and $\vec{r}_2$. However, if the differential operator yields a constant (in this case, zero) when applied to $W_{//}$, then $\nabla^2_{\perp(2)} W_{//}(\vec{r}_1,\vec{r}_2,s) = \nabla^2_{\perp(2)} W_{//}(\vec{r}_1,\vec{r}_2=\vec{r}_1,s)$ is that same constant; $\left[DV(\vec{r}=\vec{r}_2)\right]\cdot V(\vec{r}=\vec{r}_1) = \left[DV(\vec{r}=\vec{r}_1)\right]\cdot V(\vec{r}=\vec{r}_1)$. By the same reasoning, the constant is also $\left[DV(\vec{r}=\vec{r}_1)\right]\cdot V(\vec{r}=\vec{r}_2)$, and so $D_{(1)} W_{//}(\vec{r}_1,\vec{r}_2,s) = D_{(2)} W_{//}(\vec{r}_1,\vec{r}_2,s)$, implying $\nabla^2_{\perp(1)} W_{//}(\vec{r}_1,\vec{r}_2,s) = \nabla^2_{\perp(2)} W_{//}(\vec{r}_1,\vec{r}_2,s) = 0$.

Now for equation (3), which is an expansion theorem. First consider $W_{//}(\vec{r}_1,\vec{r}_2,s)$ as a function that solves $\nabla^2_{(1)} W_{//}(\vec{r}_1,\vec{r}_2,s) = 0$, where the Laplacian operator only applies to the two dimensional space $\vec{r}_1$ described with polar coordinates r_1 and ϕ_1. By the familiar separation of variables method, $W_{//}(\vec{r}_1,\vec{r}_2,s) = T(\vec{r}_2,s)\,\psi(\phi_1)\,G(r_1)$ and $\psi(\phi_1)$ = {A function of r_1 only} $cos[m(\phi_1 - \phi_1^{(n)})]$. The integer m ensures that $\psi(0)$ equals $\psi(2\pi)$. The solutions to the separated differential equation for $G(r_1)$ are $G_0(r_1) = A_0 + B_0\, ln(r_1)$ and $G_m(r_1) = A_0\, r_1^{+m} + B_0\, r_1^{-m}$ with A_i and B_i arbitrary constants. The wakefield potential is finite at $r_1 = 0$, so the B_i are zero for all i. Subsume T into the A_i, leaving $W_{//}(\vec{r}_1,\vec{r}_2,s) = \sum_{n=0}^{\infty} A_i(\vec{r}_2,s)\, r_1^m \cos\left[m\left(\phi_1 - \phi_1^{(n)}\right)\right]$.

It is at this point that we have to allow that multiple modes may have the same azimuthal order; the A_i are one-to-one mapped to solutions to the separated equation for $G(r_1)$, but there can be two $cos[m(\phi_1 - \phi_1^{(n)})]$ terms, with different $\phi_1^{(n)}$

values multiplied to each solution $G(r_1)$. Again, n indexes the modes, and m indexes the azimuthal order of the modes.

Applying the same technique to $\vec{r}_2$, and use $W_{//}^{(n)}(s)$ rather than A_i to denote the remaining functions of s,

$$W_{//}(\vec{r}_1,\vec{r}_2,s) = \sum_{n=0}^{\infty} W_{//}^{(n)}(s)\ \ r_1^m \cos\left[m\left(\phi_1 - \phi_1^{(n)}\right)\right]\ \ r_2^m \cos\left[m\left(\phi_2 - \phi_2^{(n)}\right)\right].$$

But $\phi_1^{(n)}$ equals $\phi_2^{(n)}$. Consider $W_{//}(\vec{r}_1,\vec{r}_2,s)$ when $r_1 = r_2$ but $\phi_1 \neq \phi_2$. From the explict form of equation (1) exchange of $\vec{r}_1$ with $\vec{r}_2$, or equivalently exchange of ϕ_1 with ϕ_2, will not change the value of $W_{//}$. From the expansion expression, this can only happen when $\phi_1^{(n)} = \phi_2^{(n)}$; this is the quantity ϕ_n. It will be determined by the azimuthal geometry of the cavity. For the common case where the cavity is azimuthally symmetric, the symmetry of the system is broken by the entering bunch at ϕ_2; then $W_{//}(\vec{r}_1,\vec{r}_2,s) = \sum_{n=0}^{\infty} W_{//}^{(n)}(s)\ \ r_1^m r_2^m \cos\left[m\left(\phi_2 - \phi_1\right)\right]$.

Finally for equation (4), which is essentially the Panofsky-Wenzel[13] theorem. From a Maxwell equation, $\hat{z} \times \frac{\partial}{\partial t}\vec{B}(\vec{r},z,t) = \frac{\partial}{\partial z}\vec{E}_\perp(\vec{r},z,t) - \nabla_\perp E_z(\vec{r},z,t)$ so the transverse component of the wake potential is

$$\vec{W}_\perp(\vec{r}_1,\vec{r}=\vec{r}_2,s) = \frac{1}{q_1}\int_{-\infty}^{+\infty} dz \left[E_\perp(\vec{r},z,t) + c\int dt \left\{ \frac{\partial}{\partial z} E_\perp(\vec{r},z,t) - \nabla_\perp E_z(\vec{r},z,t) \right\} \right]_{t=\frac{z+s}{c}}$$

where the subscript 2, indicating that the fields are evaluated at the trailing bunch, has been squelched. After finding the functional form of the indefinite integral, that form is to be evaluated at $t = z + s / c$, and the integration constant is to be discarded. So we can write an upper limit of $z + s / c$, and select a lower limit at some value where all the fields and their derivatives are zero. From Lebnitz' rule, $\frac{d}{dz}\int^{(z+s)/c} dt\ E_\perp(\vec{r},z,t) = \int^{(z+s)/c} dt\ \frac{\partial}{\partial z} E_\perp(\vec{r},z,t) + \frac{1}{c} E_\perp(\vec{r},z,t)$ and so

$$\vec{W}_\perp(\vec{r}_1,\vec{r}=\vec{r}_2,s) = \frac{1}{q_1}\int_{-\infty}^{+\infty} dz \left[E_\perp\left(\vec{r},z,\frac{z+s}{c}\right) + c\int^{(z+s)/c} dt\, \frac{\partial}{\partial z} E_\perp(\vec{r},z,t) - c\int^{(z+s)/c} dt\ \nabla_\perp E_z(\vec{r},z,t) \right]$$

$$= \frac{c}{q_1}\int_{-L}^{+L} dz \left[\frac{d}{dz}\int^{(z+s)/c} dt E_\perp(\vec{r},z,t) \right] - \frac{c}{q_1}\int_{-\infty}^{+\infty} dz \left[\int^{(z+s)/c} dt\ \nabla_\perp E_z(\vec{r},z,t) \right].$$

[13] W.K.H.Panofsky and W.A.Wenzel, Rev. Sci. Instr. **27** (1956) 967.

The range of the first integral is constricted into the region of non-zero fields to show why the first integral is zero. At the electric boundaries that define the integration range, $E_\perp$ is zero, and consequently

$$\int_{-L}^{+L} dz \left[\frac{d}{dz} \int^{(z+s)/c} dt E_\perp(\vec{r},z,t) \right] = \int^{(z+s)/c} dt E_\perp(\vec{r},z,t) \Big|_{z=-L}^{z=+L} = \int^{(L+s)/c} dt E_\perp(\vec{r},L,t) - \int^{(-L+s)/c} dt E_\perp(\vec{r},-L,t)$$

vanishes.

The second integral, $-\frac{c}{q_1} \int_{-\infty}^{+\infty} dz \left[\int^{(z+s)/c} dt \, \nabla_\perp E_z(\vec{r},z,t) \right] = -\frac{c}{q_1} \int_{-\infty}^{+\infty} dz \;\; \nabla_\perp A_z(\vec{r},z,t=(z+s)/c)$ is identically zero for a pure TE mode.

Again applying the Leibnitz rule,

$$\begin{aligned}
\frac{d}{ds} \vec{W}_\perp(\vec{r}_1,\vec{r}=\vec{r}_2,s) &= -\frac{c}{q_1} \frac{d}{ds} \int_{-\infty}^{+\infty} dz \int^{(z+s)/c} dt \, \nabla_\perp E_z(\vec{r},z,t) \\
&= -\frac{c}{q_1} \nabla_\perp \int_{-\infty}^{+\infty} dz \, \frac{d}{ds} \int^{(z+s)/c} dt \; E_z(\vec{r},z,t) \\
&= -\frac{c}{q_1} \nabla_\perp \int_{-\infty}^{+\infty} dz \, \frac{1}{c} E_z(\vec{r},z,t=(z+s)/c) \\
&= -\nabla_{\perp(2)} W_{//}(\vec{r}_1,\vec{r}=\vec{r}_2,s)
\end{aligned}$$

where the subscript 2 has been restored in the last expression. Re-integration gives $\vec{W}_\perp(\vec{r}_1,\vec{r}_2,s) = -\nabla_{\perp(2)} \int^{s} d\sigma \, W_{//}(\vec{r}_1,\vec{r}_2,\sigma)$, where the lower bound on the integral is omitted to indicate that we want the value of the antiderivative at a certain value of σ.

The second appendix

The convention used in the discrete Fourier transform over a finite domain is that the transform of complex sequence d_k, where k runs from 0 to (N_{IN} - *1*), is

$$D_n \equiv \sum_{k=0}^{N_{IN}-1} d_k \exp\left(-2\pi i\, kn / N_{IN}\right)$$

and the inverse transform is

$$d_n \equiv \frac{1}{N_{IN}} \sum_{k=0}^{N_{IN}-1} D_k \exp\left(+2\pi i\, kn / N_{IN}\right).$$

For continuous functions over [-∞,+∞], the Fourier transform convention is

$$\mathcal{F}[f(t)] = \int_{-\infty}^{+\infty} f(t) e^{-i\omega t}\, dt = \tilde{f}(\omega).$$

The third appendix

For a bunch train and witness bunch propagating through the cavity at fixed $\vec{r} = \vec{r}_1 = \vec{r}_2$, the longitudinal wakefield is, from equation 5,

$$W_{//}(\vec{r}, s) = \sum_n \frac{R^{(n)}}{Q} \omega_n \cos\left(\frac{\omega_n s}{c}\right)\ r^{2m} \cos^2\left[m(\phi - \phi_n)\right]$$

where the damping by external couplers is neglected because we will be considering this function over short time periods.

This expression is for point bunches. MAFIA computes the time domain evolution for specific, non-singular, charge distributions, and so the above quantity is not quite what is produced by the code. A charge density of a Gaussian longitudinal profile would be

$$\rho(\vec{r}, z, t) = q \frac{f(\vec{r})}{\sqrt{2\pi}\,\sigma} \exp\left(\frac{-\left((z - ct) - z_0\right)}{2\sigma^2}\right).$$

where z_0 = position at time zero and f gives the r-ϕ plane distribution of the bunch. However, the simulation works with $f(\vec{r}) = \delta(\vec{r})$, and it is more convenient to work with the trailing distance s, rather than with z and t. Additionally. the charge

density will be convoluted with the point-bunch wakefield and then divided by the total charge q. As a result the best thing to do with ρ, after writing it, is to ignore it. Instead work with the normalized linear charge density

$$\lambda(s) = \frac{1}{\sqrt{2\pi}\sigma}\exp\left(\frac{-(s-s_0)^2}{2\sigma^2}\right),$$

where s_0 is the distance from the center of the bunch to the origin of the s coordinate system. Perforce the origin of the s coordinate system must co-move with the bunch, but for a spatially extended bunch it can be placed quite arbitrarily at the head, tail, center, or elsewhere in the bunch. MAFIA places it at the head of the bunch. In the calculations shown here, the Gaussian bunch extended to ±5σ and so s_0 = 5σ. Therefore, the quantity produced by the finite element integration is (neglecting the contributions that are not part of the discrete modal spectrum)

$$\begin{aligned} W_{//}^{FEM}(\vec{r},s) &= \int_0^\infty d\xi\, \lambda(s-\xi) W_{//}(\xi) \\ &= \frac{1}{\sqrt{2\pi}\,\sigma}\int_0^\infty d\xi \exp\left(\frac{-(s-s_0-\xi)^2}{2\sigma^2}\right)\sum_n \frac{R^{(n)}}{Q}\omega_n \cos\left(\frac{\omega_n s}{c}\right)\; r^{2m}\cos^2\left[m(\phi-\phi_n)\right] \end{aligned}$$

where the lower bound on the integral expresses causality. The energy lost by the bunch as it passes through the structure is found from $W_{//}^{FEM}$ by treating the exciting bunch as the witness bunch: $\Delta E = q^2 k_{tot}(\vec{r}) = q^2\int_{-\infty}^{+\infty} ds\,\lambda(s) W_{//}^{FEM}(\vec{r},s)$. The total loss parameter has a definite relationship to the modal loss parameters. In the limit $\sigma \to 0$, where $\lambda(s) \to \delta(s-s_0)$,

$$\begin{aligned} \lim_{\sigma\to 0} k_{tot}(\vec{r}) &= \int_{-\infty}^{+\infty} ds\,\delta(s-s_0)\int_0^{+\infty} d\xi\,\delta(s-s_0-\xi)\sum_n \frac{R^{(n)}}{Q}\omega_n\cos\left(\frac{\omega_n s}{c}\right)\; r^{2m}\cos^2\left[m(\phi-\phi_n)\right] \\ &= \int_0^{+\infty} d\xi\,\delta(\xi)\sum_n \frac{R^{(n)}}{Q}\omega_n\cos\left(\frac{\omega_n s_0}{c}\right)\; r^{2m}\cos^2\left[m(\phi-\phi_n)\right] \\ &= \frac{1}{2}\sum_n \frac{R^{(n)}}{Q}\omega_n\cos\left(\frac{\omega_n s_0}{c}\right)\; r^{2m}\cos^2\left[m(\phi-\phi_n)\right] \end{aligned}$$

where the properties of the δ function at integration boundaries are used in the last step. The terms in the final series are the modal loss parameters,

$$k^{(n)}(\vec{r}) = \frac{\omega_n}{2}\frac{R^{(n)}}{Q} r^{2m}\cos^2\left[m(\phi-\phi_n)\right] = \frac{\left\{V_n(\vec{r})\right\}^2}{4U_n}.$$

There will also be a contribution from the continuum part of the wakefield, so $k_{tot}(\vec{r}) > \sum_n k^{(n)}(\vec{r})$; the difference is the broadband $k_{bb}(\vec{r})$.

It is also valuable to have an analytic approximation for the longitudinal wakefield in the case of a short Gaussian bunch. In the limit $\sigma, s_0 \ll s$,

$$W_{//}^{SHORT}(\vec{r},s) = \lim_{\sigma\to 0} \frac{1}{\sqrt{2\pi}\,\sigma}\int_0^\infty d\xi \exp\left(\frac{-(s-\xi)^2}{2\sigma^2}\right)\sum_n 2k^{(n)}\cos\left(\frac{\omega_n s}{c}\right)$$
$$= \frac{2}{\sqrt{2\pi}\,\sigma}\sum_n 2k^{(n)}\exp\left(\frac{-s^2}{2\sigma^2}\right)\int_0^\infty d\xi \exp\left(\frac{2s\xi-\xi^2}{2\sigma^2}\right)\cos\left(\frac{\omega_n s}{c}\right).$$

From a table of integrals, for $Re(\beta) > 0$,

$$\int_0^\infty dx\,\cos(bx)\,e^{-\beta x^2+\gamma x} = \frac{1}{4}\sqrt{\frac{\pi}{\beta}}\left\{\exp\left(\frac{(\gamma+ib)^2}{4\beta}\right)\left[1+\Phi\left(\frac{\gamma+ib}{2\sqrt{\beta}}\right)\right]+\exp\left(\frac{(\gamma-ib)^2}{4\beta}\right)\left[1+\Phi\left(\frac{\gamma-ib}{2\sqrt{\beta}}\right)\right]\right\}$$

where $\Phi(x) = -\Phi(-x)$ is the error function $2/\sqrt{\pi}\int_0^x dt\,e^{-t^2}$. In this problem, $\beta = 1/2\sigma^2$ $\approx 5.6 \times 10^6$ m^{-2}, $\gamma = s/\sigma^2 \approx 11 \times 10^6$ m^{-1} (more or less) and $b = \omega_n/c \approx 250$ m^{-1} so we need to evaluate Φ at a large value $A = \gamma/2\sqrt{\beta}$ multiplied by $(1 + i\varepsilon)$, with $\varepsilon = b/\gamma$. Using $\Phi(xy) = \frac{2y}{\sqrt{\pi}}\int_0^x dt\,e^{-t^2y^2}$ with $x = A$ and $y = (1 + i\varepsilon)$,

$$\Phi\left(A[1+i\varepsilon]\right) \approx \frac{2[1+i\varepsilon]}{\sqrt{\pi}}\left\{\int_0^A dt\,e^{-t^2} + 2i\varepsilon\int_0^A dt\,t^2e^{-t^2}\right\}.$$

For the first term, $\Phi(x)$ for large x is approximated by $1 - e^{-x^2}/x\sqrt{\pi}$, and the second term can be dropped; for the second term, substitute u for t^2 and replace the upper limit A^2 with ∞ to get $\sqrt{\pi}/4$. Then $\Phi(x) \approx 1 + 2i\varepsilon$ and

$$\exp\left(\frac{(\gamma+ib)^2}{4\beta}\right)\left[1+\Phi\left(\frac{\gamma+ib}{2\sqrt{\beta}}\right)\right]+\exp\left(\frac{(\gamma-ib)^2}{4\beta}\right)\left[1+\Phi\left(\frac{\gamma-ib}{2\sqrt{\beta}}\right)\right]$$
$$= 2\exp\left(\frac{\gamma^2-b^2}{4\beta}\right)\left[2\cos\left(b\gamma/2\beta\right)+2i\frac{b}{\gamma}i\sin\left(b\gamma/2\beta\right)\right].$$

It is tempting to drop b^2 on the grounds that it is much smaller than γ^2, but the γ^2 term will soon be canceled. Again dropping terms in b/γ,

$$\int_0^\infty dx\,\cos(bx)\,e^{-\beta x^2+\gamma x} = \sqrt{\frac{\pi}{\beta}}\exp\left(\frac{\gamma^2-b^2}{4\beta}\right)\cos\left(b\gamma\big/2\beta\right)$$

for $Re(\beta) > 0$, $b \ll \gamma$. Then

$$W_{//}^{SHORT}(s) = 2\sum_n k^{(n)}\cos\left(\frac{\omega_n s}{c}\right)\exp\left(-\omega_n^2\sigma^2\big/2\right).$$